ISEL
INSTITUTO SUPERIOR DE ENGENHARIA DE LISBOA

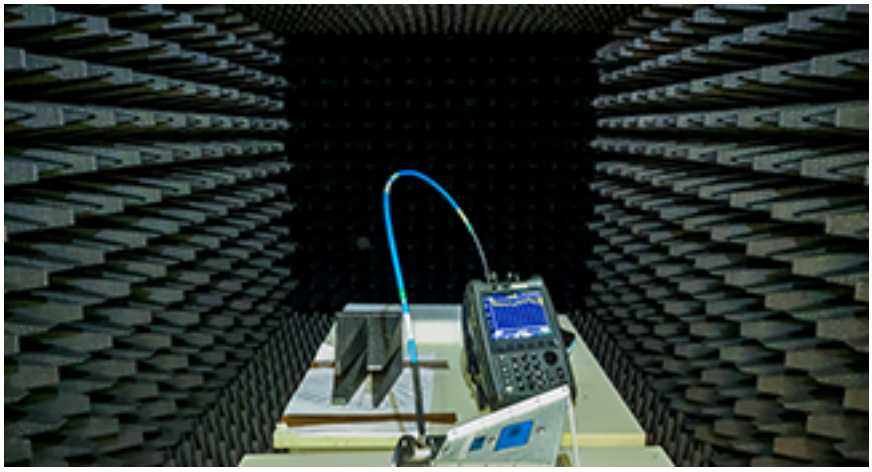

Design and Characterization of a New Absorber Material for Anechoic Chambers

Marco Filipe Coelho Anacleto

Dissertação para obtenção do Grau de Mestre em

Eletronic and Telecommunications Engineering

Orientadores: Prof. Doutor Pedro Renato Tavares Pinho
Doutor Amit Kumar Baghel

Júri

Presidente: Prof. Nuno António Fraga Juliano Cota
Vogais: Prof. Doutor Pedro Renato Tavares Pinho
Prof. Doutor António Luís Campos da Silva Topa

December 2022

Acknowledgments

First and foremost, I want to thank my advisors, Prof. Pedro Pinho, and Amit Baghel. A special thank you to them for their knowledge, motivation, criticism, praise, dedication, and professionalism. I could not have done this work without their help.

Thank the Instituto de Telecomunicações Aveiro for providing access to the software license, material, and equipment for this dissertation's absorber material measurement and development.

A special thank you to my parents, Beatriz Anacleto and Fortunato Anacleto, who have provided me with the best education through their hard-working. For supporting me in all aspects of my life, being an example of love, affection, dedication, and respect, and always motivating me to transcend all life's challenges. Thank you for allowing me to make you feel proud and happy using everything that you have taught me.

A special thank to my girlfriend, Sara Rodrigues, for all the support she gave me with unconditional love, patience, kindness, and extreme motivation, plus encouragement to complete this challenging work.

Thank to my brother Pedro Anacleto, sister-in-law Anabela and nephews André and Gonçalo for their generosity, love, and support throughout my life.

To ISEL, for all the knowledge transmitted and all the provided professional and personal experiences, without which I would never grow and be the person I am now.

Last but not least, thank to my personal friends and ISEL colleagues, particularly Rafael Matos and João Rocha, for helping me and always being there for me during the good and bad times.

To each one of you - Thank you.

Abstract

Telecommunication systems are one of the most significant pillars of industry and modern life. They are essential to provide fast and flawless communications and delivering high-quality services to users. In Radio Frequency (RF) telecommunication systems, the antenna is the interface between the radio system and the external environment, designed to radiate and receive electromagnetic waves.

Antenna measurements are fundamental for studying the antenna performance, providing their radiation pattern, gain and others. An anechoic chamber design from 1 to 12 GHz with compact dimensions (L x W x H): 0.4 X 0.4 X 0.3 m^3 is designed in this dissertation with a new type of absorber. The radiation pattern of a monopole antenna and a patch antenna was used to compare the performance of the traditional absorber material and the new type of absorber, based in Metamaterial (MM). The antenna radiation pattern and gain simulated in the compact chamber with the metamaterial have produced the same result as in free space. The results open the direction to use the metamaterial as the potential absorbing material for future chambers.

Keywords

Absorber, Antennas, Anechoic chamber, Metamaterial, Radiation pattern, Telecommunications;

Resumo

Os sistemas de telecomunicações são um dos pilares mais importantes da indústria e da vida moderna. São essenciais para fornecer comunicações rápidas, isentas de falhas, fornecendo assim serviços de alta qualidade aos seus utilizadores. Nos sistemas de telecomunicações RF, a antena é a “interface” entre o sistema de rádio e o ambiente externo, e tem como propósito a emissão e receção de ondas eletromagnéticas.

As medições das antenas são fundamentais para estudar o desempenho da mesma, fornecendo dados como o seu diagrama de radiação, ganho, entre outros. É apresentada nesta dissertação, uma câmara anecoica compacta, projetada para o intervalo de frequências compreendido entre 1 e 12 GHz cujas dimensões são (L x C x A): 0,4 X 0,4 X 0,3 m^3 contendo um novo tipo de material absorvente. Foi utilizado o diagrama de radiação de uma antena monopolo e de uma antena ”patch” para comparar o desempenho do material absorvente convencional com o desempenho de um novo absorvente baseado em metamaterial. O diagrama de radiação da antena e o ganho, simulados na câmara compacta, com o metamaterial produziram um resultado semelhante ao obtido em espaço livre. Os resultados abrem assim a possibilidade de se usar o metamaterial como um potencial material absorvente em futuras câmaras.

Palavras Chave

Antenas, Câmara anecoica, Diagrama de radiação, Material absorvente, Metamaterial, Telecomunicações;

Contents

List of Figures

List of Tables

Acronyms

1G	1^{st} Generation of Mobile Telecommunications System
2G	2^{nd} Generation of Mobile Telecommunications System
3G	3^{rd} Generation of Mobile Telecommunications System
4G	4^{th} Generation of Mobile Telecommunications System
5G	5^{th} Generation of Mobile Telecommunications System
AC	Anechoic Chamber
AUT	Antenna Under Test
CATR	Compact Antenna Test Range
DUT	Device Under Test
EM	Eletromagnetic
EMC	Eletromagnetic Compatibility
GO	Geometrical Optical
GSM	Global System for Mobile Communication
HARP	Halpern AntiRadar Paint
IT	Instituto de Telecomunicações
ITO	Indium Tin Oxide
MIMO	Multiple-Input Multiple-Output
MM	Metamaterial
PET	Polyethylene terephthalate
PIM	Passive Intermodulation
QZ	Quiet Zone
RCS	Radar Cross Section
RF	Radio Frequency

VSWR Voltage Standing Wave Ratio

1

Introduction

Contents

This chapter introduces the topic of this dissertation, related to the absorber material for Anechoic Chambers (ACs). The structure of this chapter stands organized with a motivation section including first AC builds and their uses, followed by an overview of AC settings and components, the proposed objectives to be accomplished, the document outline, and finishing with the related publications from this work.

1.1 Motivation

At the end of the 19^{th} century, Guglielmo Giovanni Maria Marconi performed the first successful radio communication between two locations using the wireless telegraph. Since this significant history of wireless telecommunications, wireless communications have started a massive evolution. While at Motorola in the 1970s, Marty "Martin" Cooper, an american engineer, invented the first handheld cellular mobile phone, which marked the beginning of a new and essential technology era. Mobile communications allow for a wide variety of services, resulting from evolution over more than 40 years, starting with the launch of 1^{st} Generation of Mobile Telecommunications System (1G), known as analog mobile communication. The 2^{nd} Generation of Mobile Telecommunications System (2G) emerged in the late 1980s and introduced the new and successful technology known as Global System for Mobile Communication (GSM), which was responsible for the start of the digital mobile network era, reducing costs compared to the previous generation. In 2000, the 3^{rd} Generation of Mobile Telecommunications System (3G) introduced video calls and more bandwidth for data packets. In 2008 the 4^{th} Generation of Mobile Telecommunications System (4G) improved the mobile data capacity and speed and allowed the use of many advanced multimedia services, such as social networks. Nowadays, the 5^{th} Generation of Mobile Telecommunications System (5G) aims to surpass the 4G limits and bring lower latency with increased speed and capacity. These features are attainable using Multiple-Input Multiple-Output (MIMO) to grant better signal and aptitude to transmit and receive from multiple directions. Mobile network systems, such as mobile phones, can be very complex due to the device's capacity to process a high volume of information flows. These systems can handle more than one radio system with different frequency ranges. The AC grants the suitable environment to measure these systems using appropriate absorbing material characteristics for the desired frequency. In 1953, appear the first commercially available microwave absorbers, and in the same year, the first AC to be used for antenna tests and measurements. Previously, absorber material and AC were for the use of the army. The most significant research in AC and microwave absorbing materials occurred in recent years with the use of Metamaterial (MM) structures for wideband reduction of antennas Radar Cross Section (RCS). Absorbent material design is decisive in the performance of the AC, so one of this dissertation's motivations is to design a new absorber that increases the performance of an AC.

1.2 Topic Overview

When developing a new antenna, it is important to establish rules to make systems work perfectly and prevent radiation spread over undesired directions. An AC is a shielded room with radio-wave absorbing material applied to the walls, ceiling, and floor to grant precision measurements inside it. It is a Radio Frequency (RF) free-space simulator ideal for conducting impedance measurements on antenna systems, absorbing reflections inside the chamber, and also preventing external sources from being able to penetrate the AC. The absorbers inside the chamber are often pyramidal, which brings advantages compared with other designs due to their wide frequency and incident angle characteristics to absorb arbitrary incoming Eletromagnetic (EM) waves from Antenna Under Test (AUT). There are other available absorbers, but pyramid-shaped absorbers are the most used. The existing evolution of computational capacity makes the planning of ACs backed up by EM simulators possible, which provides higher reliability to the final product.

1.3 Objectives

The main goal of this dissertation is to present the design and analysis of a new absorber design for AC use for frequency ranges above 1 GHz, which could achieve better results than the currently used absorbent materials. It is vital to collect all information about the AC state of the art required to understand the science of absorber material. The following procedure is to simulate the design in the appropriate software as CST Studio Suite [1]. For the final steps, after obtaining simulation results, use the new format to cover an AC and perform the measurements to compare the performance between the standard and new absorber design by simulation. And if it is possible to produce the new absorber design, and test it in the laboratory.

1.4 Outline

This dissertation is divided into five chapters arranged as follows: Chapter 2 provides a technical introduction to important antenna parameters, the general concepts about ACs and an overview of the existing and most used types of ACs and the use cases, sorting them by size, format, and types of absorber material. Chapter 3 introduces absorber design comparison using simulation software and the research about a new absorber design and how it performs compared with the standard formats. Chapter 4 describes the characterization of a rectangular AC covered with the newly developed material from chapter 3. Finally, Chapter 5 provides the main conclusions, as well as future work is suggested.

1.5 Publications

The following scientific paper was written in the context of this work:

- ”Novel Ultra-thin Meta-Material Absorber for Potential Use in Compact Anechoic Chamber” submitted by Marco Anacleto (ISEL - DEETC), Amit Baghel (IT Aveiro), Pedro Pinho (UA and IT Aveiro) and Nuno Borges Carvalho (UA and IT Aveiro). This paper was submitted and accepted to the 17th European Conference on Antennas and Propagation (EuCAP 2023 Florence Italy - March 2023).

2

Anechoic Chambers Overview

Contents

This chapter introduces the target parameters that a project designer must address when planning a new AC. Section 2.1 presents an overview about AC, and their applications, Section 2.2, introduces some EM types of measurements, Section 2.3 explains the difference between indoor and outdoor measurements, Section 2.4 describes the main antenna measurement parameters. Section 2.5 presents the most used antenna ranges in measurements. The chosen approach is the indoor far-field range as defined in Section 2.5.1. Furthermore, this chapter also includes AC use cases for each type. Section 2.6 shows important aspects about rectangular ACs and the use cases, Section 2.7 describes the tapered ACs, comparing with the rectangular types, and their use cases, Section 2.8 presents the available AC absorbers and their frequency range effect for each type, and lastly section 2.9 presents some papers regarding AC development as design and absorber types.

2.1 Anechoic Chamber Overview

Nowadays, telecommunications have quite powerful functions, allowing communication at high-speed rates and interaction with many services simultaneously. Enhancing these services is challenging, requiring hardware and software to handle such operations. The hardware responsible for wave propagation requires multiple measurements to certify its functionalities, offering system performance as well. There are several EM field measurements to verify the quality of the radiant hardware, such as the antenna pattern measurement, radiated emission measurement, radiated susceptibility measurement, Eletromagnetic Compatibility (EMC) measurement, and RCS measurement. Those measurements require an ideal test environment, shielded and controlled internal wave reflections. ACs can fulfill these requirements by providing a no-echo environment simulating the free space, reducing the effects of these undesired signals during the tests, and costs, compared with an outdoor range. The antenna measurements deliver information about the performance of a selected antenna, which can be in far-field or near-field range. For instance, to comprehend whether the power is radiating and if in the desired direction as planned in the design specifications, and no less important to measure how much power is in undesired directions. For the planning and construction of an AC, it is necessary to know the antenna behavior and the parameters to choose the right chamber type, providing the best performance for the lowest cost. It is crucial to properly define the AC size for specific antenna sizes and the test frequencies. The absorber inside the chamber is the key to reducing reflected waves and increasing the quality of the measurements. The absorber material is selected to absorb the energy of the waves efficiently and transform that energy into heat. All inside walls must be fully covered with the absorber material to avoid reflections with a higher power. Therefore, the measurement of EM properties of an electronic device is required to determine the stimulation of a device by radio waves, perform a test of immunity, and measure device-produced radiations.

2.2 Types of Electromagnetic Measurements

This section describes the main concerns in EM measurements and their importance for implementation.

2.2.1 Radiation Measurements

The radiation measurements became very important in the past years, not only because of health concerns but also to guarantee the correct operation of the systems, ensuring that laws about radiation power limits are satisfied. Calibration is essential to avoid errors, keeping these components within the required parameters. This type of measurement includes antenna pattern measurement, defined as ”the spatial distribution of a quantity that characterizes the EM field generated by an antenna” [2]. A pattern is a radiation map, usually a 2D or a 3D representation.

2.2.2 Compatibility Measurements

The EMC defines the electronic device limit tolerance to EM radiation. There are two ways to reach the equipment's EMC. The first one is to control sources lowering their emissions, and the second one is to increase the immunity of equipment that may be affected. Decreasing emissions and increasing immunity could create a high cost to industry, slowing down new technology evolution. Balancing this is not easy, although the industry warns consumers about equipment cautions and restrictions to prevent malfunctions and ensure human radiation exposure safety.

2.2.3 Susceptibility Measurements

Susceptibility measurements need a shield AC due to the required high power levels to generate the necessary fields to test the susceptibility of a device to many EM field levels. The design has to be designed accurately due to minimizing uncertainty in measurements. The most critical parameter in susceptibility measurements is the uniformity of the field illuminating the Device Under Test (DUT) [3].

2.3 Measurement Environment

The EM field measures should be performed in an ideal test environment, in which there are two basic types of measurement environment approaches, the outdoor and indoor measurements. Indoor antenna measurements are performed in a controlled laboratory condition, an ”echo-free” environment or chamber, known as AC. Chambers can change into diverse sizes and shapes following the measurement purpose. Outdoor antenna measurements are performed when the measurement site requires a

clear obstruction space, within an elliptical boundary when necessary, covered with performance absorbers [4]. Outdoor measurements are suitable for measuring site attenuation and need to set up a plane wave of uniform amplitude to illuminate the test antenna, which is a mandatory requirement for determining far-zone performance [5].

2.4 Antenna Measurements

Antenna measurements are essential to understanding antenna behavior for a given system. Antennas stand responsible for receiving and sending radio waves. The IEEE standard designates an antenna as: ”that part of a transmitting or receiving system designed to radiate or to receive EM waves” [2]. The goal is to determine how these waves propagate around the antenna. The far-field radiation region is the region of interest for this dissertation. The EM field can be measured in the AC and mapped using computational resources. This map is the radiation pattern, as mentioned before. The antenna pattern has some fundamental parameters for the antenna designer to consider, such as gain, beamwidth, side-lobe levels, front-to-back ratio, and polarization [6].

2.4.1 Gain

Antenna gain is the ratio of the radiated intensity in a given direction and the radiation intensity, if the power accepted by the antenna, was emitted isotropically. The gain as radiated power is a function of direction, and the terms used in this gain can be maximum gain, peak gain, or absolute gain of an antenna. When it is referred to as a specifically given polarization, divided by the radiation intensity, and the power accepted was radiated isotropically, this is called the partial gain. Realized gain is the gain of an antenna reduced by its impedance mismatch factor. Directivity is the ratio of radiation intensity in a given direction from the antenna to the radiation intensity averaged over all directions. Figure 2.1 illustrates the gain definitions described above [7].

There are different approaches to measuring gain, in which absolute gain measurements based on the Friis transmission equation are given by:

$$P_r = P_{in} G_A G_B \left(\frac{\lambda}{4\pi r} \right)^2 \tag{2.1}$$

In Equation (2.1), P_r , is the received power, and P_{in} is the power into the antenna that is transmitting. If the two antennas have G_A = G_B, they are identical, with distance information r and wavelength λ, and the gain of the antennas results from the transmitted and received powers. The Friis equation makes the relation between two antennas in free space and cannot be used in ranges without a free-space condition.

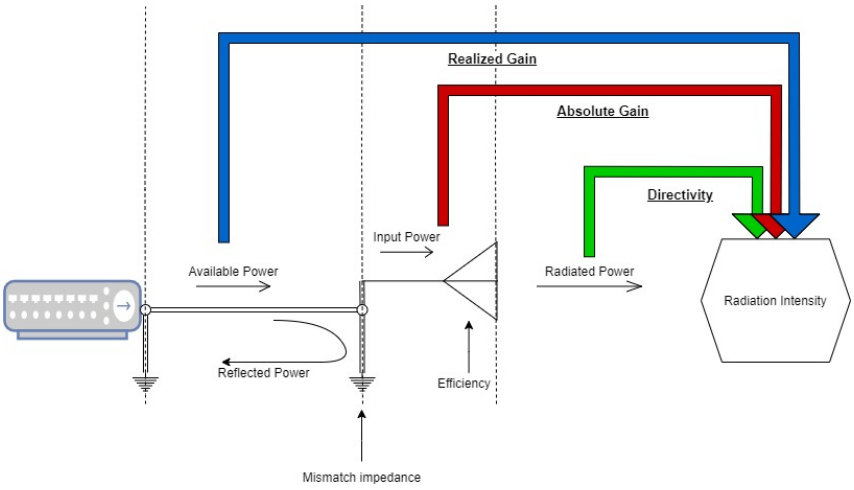

Figure 2.1: Concepts of realized gain, absolute gain, and directivity diagram, adapted from [6].

In general, the antenna measurement ranges depend on reference gain methods, where an antenna under test G_T results by comparison between its received power to the power received by a known antenna with known gain G_S, for example, and the typically used pyramidal horns [8] or dipoles.

Another method to calibrate gain standards is extrapolation ranges, presented in [9, 10], where the antennas are moved away from each other, and the data is collected with distance using a polynomial curve.

2.4.2 Beamwidth

As defined in [7], beamwidth is the angle between the two directions in which the radiation intensity is one-half the maximum value as measured along lines equidistant from the face of the antenna. The main lobe has the direction of the maximum radiation, and the side lobes are the radiation in other directions.

Figure 2.2 illustrates the concepts of beamwidth, as well as the main and side lobes.

2.4.3 Polarization

The polarization properties of fields and antennas are one of the main concerns in communication between antennas. The explanation for studying antenna polarization is the requirement for power transfer efficiency between antenna mensuration [12]. There are three forms of polarization, linear, circular, and elliptic. Linear polarization is the most used type and unfolds in vertical and horizontal polarization. Horizontal polarization is when the antenna's electric field is parallel to the earth's surface, and vertical polarization is when this field is perpendicular to the earth's surface. Circular polarization unfolds too, but in right-handed and left-handed, the right or left depends on the rotation of the polarization plane in a circle when a complete revolution occurs as the period of the radiation frequency. Elliptical polarization is

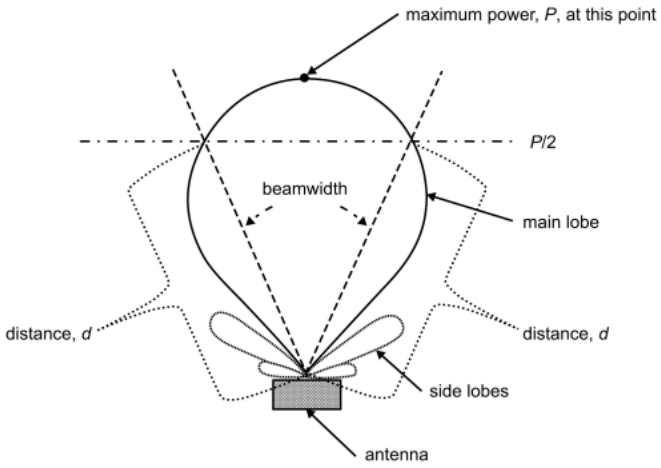

Figure 2.2: Main lobe, side lobes and beamwidth illustration schematic, adapted from [11].

a complex combination of linear and circular polarization and results from the electric field not having the same magnitude and having an arbitrary phase difference. Cross polarization is the polarization orthogonal to the desired polarization, fitting perfectly for circular polarization. Although, for linear or elliptical polarization, the direction of the reference polarization must still be defined [13]. An antenna is never 100% polarized in a single mode (linear, circular, etc.). Hence, two radiation patterns of an antenna are presented as the co-pol (or desired polarization component) radiation pattern and the cross-polarization radiation pattern [14]. Figure 2.3 shows a visual understanding of the types of antenna polarization explained before.

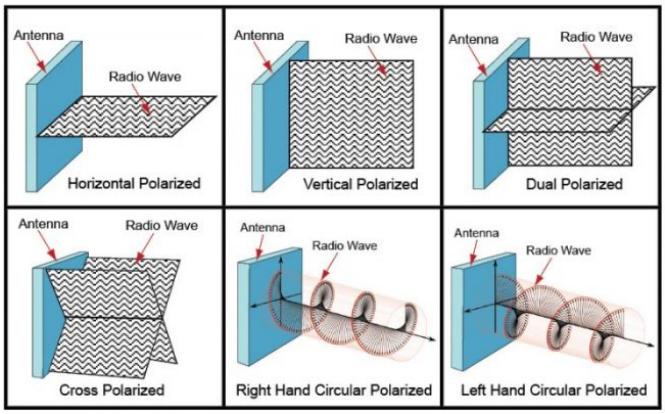

Figure 2.3: Antenna polarization explained graphically, adapted from [15].

2.5 Antenna Ranges

There are several methods for measuring the radiation patterns of antennas indoors. The options are near-field ranges, far-field ranges, and compact ranges. No single solution is ideal for all types of antennas and situations.

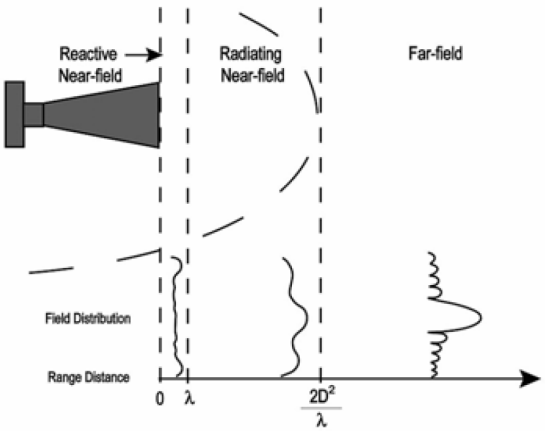

Figure 2.4: Fields of a Radiating Antenna, adapted from [16].

2.5.1 Far-field Ranges

Far-field measurements represent the best option for measuring the amplitude or phase characteristics of the DUT. Usually, on a far-field range, transmitter and receiver antennas are separated by enough distance to simulate the designated operating environment. To be in the far-field region, the distance R between the source antenna and the AUT has to satisfy the following equations:

$$R > \frac{2D^2}{\lambda} \tag{2.2}$$

$$R >> D \tag{2.3}$$

$$R >> \lambda \tag{2.4}$$

where, D is the maximum linear dimension of the antenna, and λ is the wavelength. At the distance R from eq. (2.2), the wavefront is near equal phase across the measurement area because the phase change is less than 1/16 of a wavelength, or 22.5° [16]. With this radiated pattern plane wave approximation, it is possible to collect acceptable antenna measurements. An indoor far-field range controls more precise reflections inside an anechoic chamber. It is sufficient for short far-field distances, providing security measures and protection from the weather.

2.5.2 Near-field Ranges

Near-field test ranges are usually indoor configurations with less space used. This range uses a small probe RF antenna scanned over a surface surrounding the test antenna. The near-field antenna measurements are made in the radiating near-field region, as illustrated in Figure 2.4. The range lengths are very short, to the point where the probe nearly touches the AUT. While taking measurements, near-field phase and amplitude information is collected over discrete matrix points and then transformed to the far-field using a Fourier transform, transforming the resulted data as other regular far-field antenna measurements.

2.6 Rectangular Anechoic Chambers

The rectangular anechoic chambers are the most used and easy to implement indoor far-field compared with a sphere or an ellipsoid design. These chambers also have some limitations, such as the reflectivity of the lateral walls. Lateral walls need to be covered with high-performance absorbers to reduce these limitations. In this type of chamber, illustrated in Figure 2.5, the antenna range is at a defined height, and the AUT is at the same elevation at a certain distance. Following equation 2.2 from Section 2.5.1, the distance between antennas should be the far-field distance of the AUT. There are no concerns about ground reflections indoors compared to the outdoor far-field because they are treated with RF Absorber, covering the ceiling, walls, and ground of the chamber.

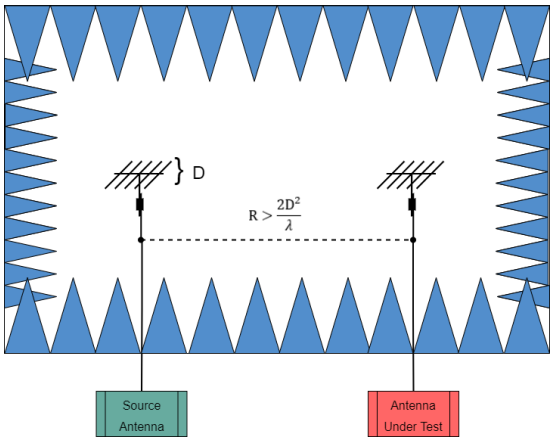

Figure 2.5: Rectangular Anechoic Chamber.

The first objective of designing a new chamber to perform measurements is understanding the acceptable error and uncertainty. The acceptable error is related to what levels of reflected energy from the absorber surfaces entering the Quiet Zone (QZ) are suitable to meet that error level. The answer about the acceptable error using the physical optics approach needs a two-dimensional chamber analysis to

reduce the complexity. Assuming a QZ of diameter D and a range antenna located at distance R inside a rectangular room with a length L, a width W, and the center of the QZ placed at a distance of C from the closest end wall. A limited number of reflected rays bounce off the walls and enter the QZ as reflected energy as shown in Figure 2.6. Starting with the rays that reflect off the end wall opposite the range antenna labeled as ξ and ζ.

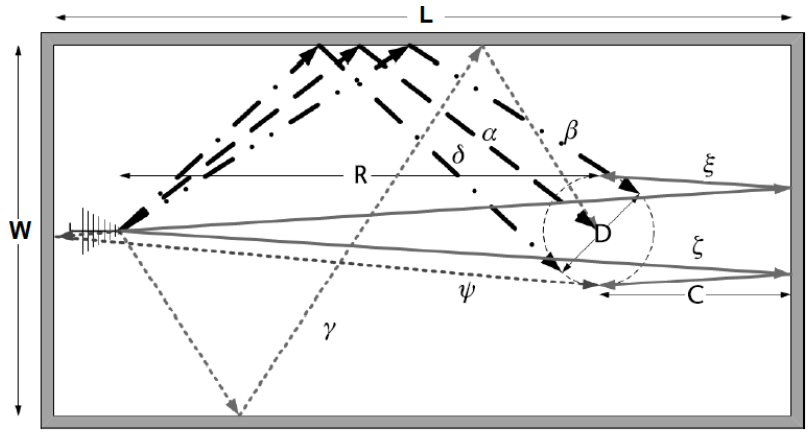

Figure 2.6: Sample of the reflected paths in a rectangular AC, adapted from [6].

The angle of incidence of these rays onto the end wall is given by [6]:

$$\varphi_\xi = \varphi_\zeta = \tan^{-1}\left(\frac{\frac{D}{2}}{R+2C}\right) \tag{2.5}$$

where φ_ξ is the angle of incidence of ray ξ and φ_ζ is the angle of incidence of ray ζ. Equation 2.5 can be modified introducing the far-field distance equation 2.6,

$$R = \frac{2D^2}{\lambda} \tag{2.6}$$

substituting:

$$\varphi_\xi = \tan^{-1}\left(\frac{\frac{D}{2}}{\frac{2D^2}{\lambda}+2C}\right) \tag{2.7}$$

If $R >> C$ the equation 2.7 can be approximated as:

$$\varphi_\xi = \tan^{-1}\left(\frac{\lambda}{4D}\right) \tag{2.8}$$

Lastly in terms of electrical size, such that $D = n\lambda$; then equation 2.8 is shortened to:

$$\varphi_\xi = \tan^{-1}\left(\frac{1}{4n}\right) \tag{2.9}$$

It is important to note that equation 2.9 is an approximation to simplify the analysis. Giving wavelength values using equation 2.9 as can be seen in Table 2.1, can be concluded that if AUT or QZ is more than two wavelengths in size (for n $\geq$ 2), then φ_ξ is smaller than 10°. The reflectivity of the absorber changes very little for angles of incidence smaller than 10°. Hence, the reflected energy level from the back wall entering the QZ will be similar to the normal incident reflectivity of the absorber.

n Wavelengths (λ)	φ_ξ(deg)
0.25	45
0.5	26.56
0.75	18.43
1	14.03
2	7.12
3	4.76
4	3.57
5	2.86

Table 2.1: Angle of incidence on the end wall versus electrical QZ size (in wavelengths λ)

Observing Table 2.1 it is noticed that for a $\frac{\lambda}{4}$ antenna, the angle of incidence on the back wall is 45°, which is greater than the 10° limit for the reflectivity of the absorber for normal incidence. Nevertheless, the previous Equation (2.9) was the result of approximations and is not showing the exact result. To test the $\frac{\lambda}{4}$ the Equation (2.2) will now be considered, and C may be at least 2λ, substituting in Equation (2.7) will result as:

$$\varphi_\xi = \tan^{-1}\left(\frac{\frac{(\frac{\lambda}{4})}{2}}{\frac{4(\frac{\lambda}{4})^2}{\lambda}+2\lambda}\right) \tag{2.10}$$

Equation (2.10) results in $\tan^{-1}\left(\frac{1}{18}\right) = 3.18°$, smaller than the 10° assuming a normal incidence reflectivity level as reported by the absorber manufacturers.

Ray Ψ is the reflected ray from the source antenna end wall that reflects toward the QZ. The source antenna, usually, is placed close to the wall and, in some cases, is mounted onto the wall. The angle of incidence for ray Ψ is given by:

$$\varphi_\Psi = \tan^{-1}\left(\frac{\frac{D}{2}}{R}\right) \tag{2.11}$$

Equation (2.11) is similar to Equation (2.5) after applying Equation (2.2). Hence, φ_Ψ is smaller than 10°, so that wall contribution to the reflectivity is the normal incidence as well.

Ray γ is the only ray in Figure 2.6 that has more than one bounce before reaching the QZ, and both rays, γ and α cross the center of the QZ. The angle of incidence for ray γ is given by:

$$\varphi_\gamma = \tan^{-1}\left(\frac{R}{2W}\right) \tag{2.12}$$

The angle of incidence for ray α is given by:

$$\varphi_\alpha = \tan^{-1}\left(\frac{R}{W}\right) \tag{2.13}$$

Observing Equation (2.12) and Equation (2.13) the conclusion is that the tangent of φ_γ is half of the tangent of φ_α. Hence, the reflectivity of the absorber for φ_γ is smaller than the reflectivity for φ_α. As ray γ goes through two bounces, the magnitudes of the rays are $|\Gamma_\alpha|$ for the single-bounce and $|\Gamma_\gamma^2|$ for the two-bounce. Since the absorber typically $|\Gamma| < 1$, it heeds that the magnitude of ray α is larger than the magnitude of ray γ. The definition of QZ level is the highest level of reflected energy entering the QZ. Therefore, arise an acceptable approximation to ignore the second-order bounces.

The remaining two rays are β and δ. The angle of incidence for ray δ is given by:

$$\varphi_\delta = \tan^{-1}\left(\frac{R - (\frac{\sqrt{2}}{2})D}{W + \sqrt{2}D}\right) \tag{2.14}$$

The angle of incidence for ray β is given by:

$$\varphi_\beta = \tan^{-1}\left(\frac{R + (\frac{\sqrt{2}}{2})D}{W - \sqrt{2}D}\right) \tag{2.15}$$

Thus, after knowing all the angles of incidence equations, it is evident that $\varphi_\delta > \varphi_\alpha > \varphi_\beta$. Generally, $R >> 0.707D$ and also $W > 1.414D$, using φ_α as the angle of incidence onto the QZ for far-field rectangular chambers is a reasonable approximation to acquire the predicted QZ level. Subsequently, the most meaningful conclusion is that for a rectangular far-field chamber, the widest angle of incidence for a single-bounce ray is the specular bounce from the lateral surfaces. Hence, the lateral surfaces of the rectangular chamber are the most influential.

2.6.1 Sizing the Rectangular Anechoic Chamber

The indoor far-field chambers are usually limited to five wavelengths in physical size antennas, corresponding to the largest physical antenna at the lowest frequency of operation. There are numerous approaches in the industry, with the most famous that the width and height of the chamber should be three times the diameter of the QZ [17]. This dissertation analysis will apply simple and flawless trigonometry to avoid invalid methods. Thus, an equation based on the far-field distance will be developed for the size of the chamber, following the parameters illustrated in Figure 2.7. The length L equation can be given by:

$$L = R + C + L_a + S_a \tag{2.16}$$

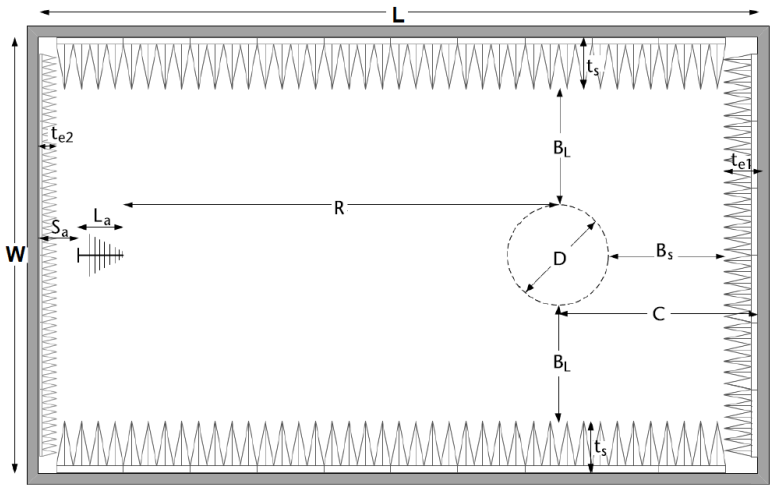

Figure 2.7: Rectangular AC with size variables, adapted from [6].

The distance between the center of QZ and the absorber base can be written as:

$$C = \frac{D}{2} + t_{e1}\lambda + B_s \tag{2.17}$$

It is crucial to verify a minimum spacing of 2λ between the AUT and the tips of the absorber (B_s) to avoid loading of the AUT at the lowest frequency [17]. Assuming that as the frequency increases, the electrical size of the antenna remains constant or smaller and that the antenna's physical size is reduced. Using the far-field criteria Equation (2.2), and the lowest frequency of operation, the equation for chamber length (L) is rewritten by:

$$L = \left(2n^2 + \frac{n}{2} + 2\right)\lambda + t_{e1}\lambda + L_a + S_a \tag{2.18}$$

The width (W) is given by:

$$W = (t_s\lambda) + n\lambda + 2B_L \tag{2.19}$$

It is possible to write the chamber size based on the desired angle of incidence and the QZ level. Following the angle of incidence from Equation (2.13), it is feasible to determine an adequate angle of incidence to provide a good absorption. Assuming that the angle of incidence is from the tip, Equation (2.13) is now given by:

$$\varphi_\alpha = \tan^{-1}\left(\frac{R}{D + 2B_L}\right) \tag{2.20}$$

Considering the far-field condition and the electrical size of the QZ, the equation is given by:

$$\varphi_\alpha = \tan^{-1}\left(\frac{2n^2\lambda}{n\lambda + 4\lambda}\right) \tag{2.21}$$

Thus, the equation for sizing the chamber based on the desired angle of incidence and the QZ level as the B_L is written by:

$$B_L = \left(\frac{2n^2 - n \tan \varphi_\alpha}{\tan \varphi_\alpha} \right) \lambda \tag{2.22}$$

Therefore, the space designated by B_L is a function of the angle and the electrical size of the AUT. These equations allow the design of a rectangular chamber based on custom parameters, such as frequency, antenna size, and space limitation.

2.7 Tapered Anechoic Chambers

The tapered anechoic chamber is the solution for the low-frequency limitations experienced with rectangular chamber types, below 300 MHz, when the wavelength is 1 meter or more. At this frequency, the absorber size needed has to be three wavelengths larger, about 3 meters, and this size of the absorber is not easy to get or cheap. The longest pyramidal absorbers manufactured are about 2.95 m size length. This solution was presented in 1965 when Emerson's paper was published [18], where he points out predominant error sources from antenna measurements, like walls, floor, and ceiling. Emerson created a new design for anechoic chambers filed a patent in 1964, in the shape of a pyramidal horn, with a large rectangular test region, illustrated in Figure 2.8.

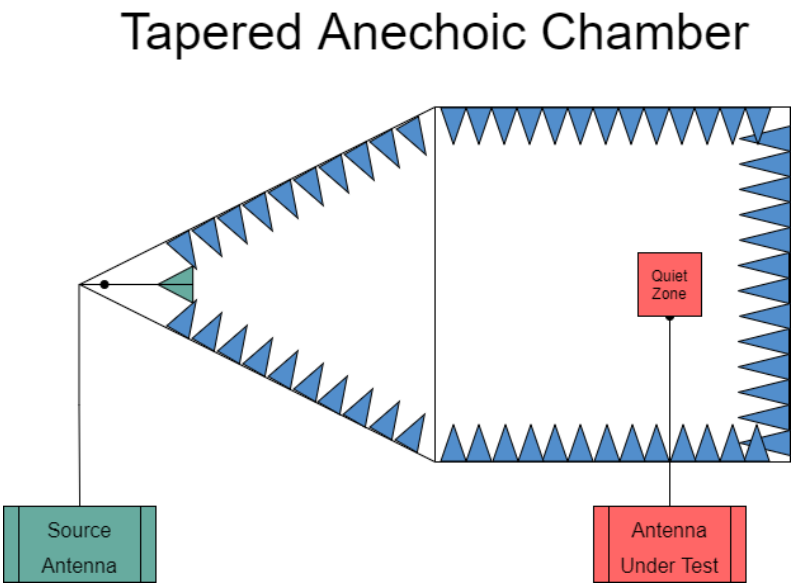

Figure 2.8: Tapered Anechoic Chamber.

When Emerson described this new design, he did not have a formulated theory for that, providing three possible explanations. The first method and the most common based on Geometrical Optical (GO) or ray-tracing; the second is an antenna theory that considers the tapered chamber as a large horn

with lossy surfaces that attenuate higher orders; and the third as a four orthogonally combined ground reflection ranges.

The GO model shows that in the tapered AC, the specular region has moved using the reflected rays to illuminate the QZ. In Figure 2.9, reflections from the side walls must be minimized for a traditional rectangular antenna chamber, as they combine with the direct illumination to create a wave across the QZ.

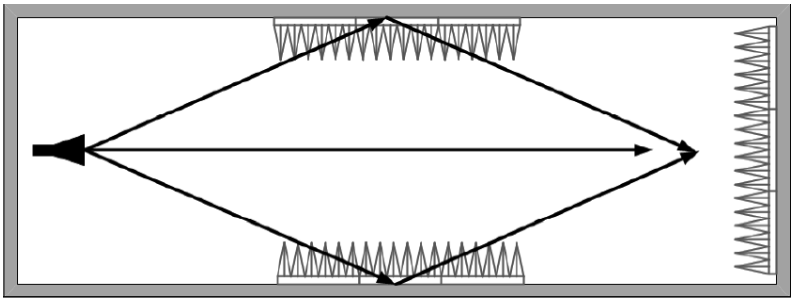

Figure 2.9: Rectangular Anechoic Chamber Reflections, adapted from [6].

In Figure 2.10, the chamber has been shaped in a tapered form, and the specular region has moved closer to the antenna. If adequately shaped, the reflected and the direct rays are parallel, helping the illumination of the QZ.

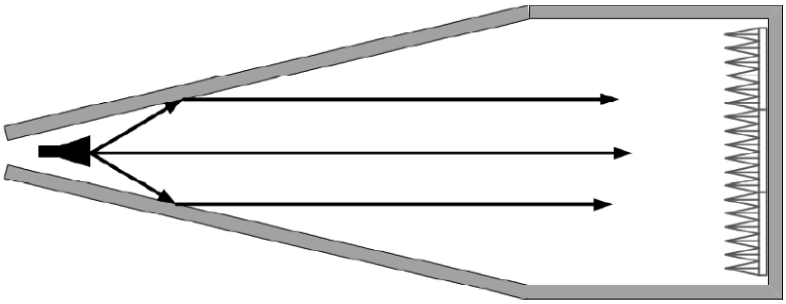

Figure 2.10: Tapered Anechoic Chamber Reflections, adapted from [6].

The GO theory tells that, since the paths of the reflected and the direct ray are very close, the phase is also very close. That might not be true following the EM basics, as the tapered section is always treated with an absorber, and the reflected signal also has a phase shift related to the properties of the absorber. Even if not treated, the reflection of a metal surface will have a 180º phase shift for some polarization. In other words, ray tracing is the key to explaining some areas of tapered chamber design, and GO theory is the key to comprehending the purpose of keeping a constant angle on the tapered section. For the ground reflection method, the approach is to look at the behavior of the tapered chamber by looking at the source or target antenna and its reflections or images. The method helps show that as the distance from the target antenna to the walls of the tapered increases, a large wave can be inserted

into the QZ field distribution. The last approach method is the array of sources theory, which also uses image theory, although it processes the images as elements as an array of sources.

2.7.1 Sizing the Tapered Anechoic Chamber

The sizing of the tapered chamber is based on empirical results as many other parameters of this chamber, also described in [19]. The first concern is the size of the QZ, which must be large enough to include the larger AUT. Likewise, in the rectangular chamber, the electrical size for the larger antenna should be limited to 5λ, remembering that the tapered chamber is a far-field range as well. The rectangular section encloses the QZ composed of lateral walls and one end wall. The end wall specifies the reflectivity of the QZ. High-performance ending wall absorbers can ensure good chamber accuracy for low frequencies. The parameters are illustrated in Figure 2.11.

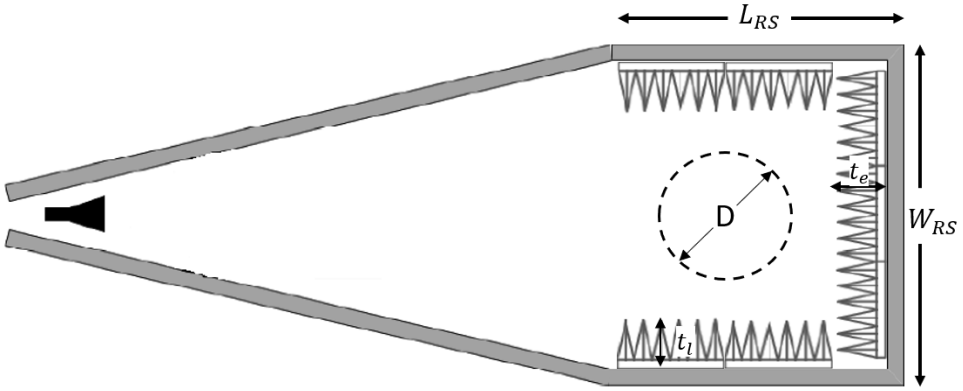

Figure 2.11: Tapered AC with size variables, adapted from [6].

The width and height of the rectangular section are given by:

$$W_{RS} = H_{RS} = D + 4\lambda + 2t_l\lambda \tag{2.23}$$

Where W_{RS} is the width of the rectangular section, and H_{RS} is the height. $t_l\lambda$ is the thickness of the end wall absorber, typical pyramidal absorber height in terms of wavelengths, and D is the diameter of the QZ. Considering the two-wavelength spacing between the QZ and the tips of the absorber.

The length of the rectangular section is written as:

$$L_{RS} = D + 4\lambda + 2t_e\lambda \tag{2.24}$$

Where $t_e\lambda$ is the electrical size of the end wall pyramid treatment plus the two-wavelength spacing.

An old approach can be found, using the width and height as three times the QZ [6]:

$$W_{RS} = H_{RS} = 3D \tag{2.25}$$

The tapered section is the critical part of the tapered chamber. Hemming in [20] states that for the operation to high frequencies, the angle of the taper should not exceed 30°. Hence, taper section length can be acquired from the equation:

$$L_{taper} = 2W_{RS} \tag{2.26}$$

2.8 Anechoic Chambers Absorbers

The AC goal is to create a volume inside where any reflected energy from its inside walls (ceiling, side walls, and floor) will be much lower than any from the direct path of the antenna tested. This volume is known as the QZ. The energy level reflected must be several dB below the direct path between the transmitting and receiving antennas. The antenna that measures the AUT is placed in the QZ to measure the direct path transmission. The AUT can also rotate, and that will cause its main beam to illuminate different surfaces of the chamber to measure the level of the field radiated by the AUT along the direct path in other directions, as shown in Figure 2.12.

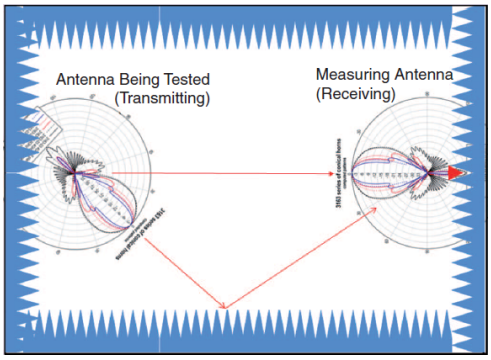

Figure 2.12: Indoor range, showing one of the reflected paths and the direct path between the AUT and the source antenna, adapted from [17].

The absorber material cannot absorb all the energy, and the measured antenna will receive part of this unabsorbed reflected energy. If the reflected energy level is higher than the energy radiated along the direct path, the radiation pattern cannot be measured accurately. The absorber needs to cut down the reflected wave at least 20 dB to 30 dB less than the incident wave to avoid errors in the measured pattern [17]. Absorbing materials have a large tapered region to reflect the incident wave and guide them inside it. The purpose is to convert the EM energy into heat. The electrical thickness of the material specifies how much energy can be absorbed. The reflection level at a normal incidence can be

approximated by equation 2.27 [17]:

$$R_o(t) = -13.374ln(t) - 26.515 \tag{2.27}$$

Where t is the thickness in wavelengths, and $0.25 \leq t \leq 20$. This approximation can be used to get a conservative value of the reflectivity of the absorber for a given thickness. For oblique incidence, the reflectivity of the absorber is in the bistatic direction. Backscattering occurs when the distance between the pyramidal tips is $\geq \lambda$ [17]. The most common materials used in absorbers are polyurethane or polystyrene foam, and a proper amount of conductive substance can be mixed with absorber material to improve performance.

2.8.1 Absorbing Materials Origin

The first known EM absorber was created in the Netherlands by Naamlooze Vennootschap Machinerieen in the mid-1930s and was a quarter-wave resonant type for the 2 GHz region [4]. It was the first known absorber employing carbon black to achieve dissipation and TiO2 (Titanium Dioxide) to achieve a high dielectric constant to reduce thickness. World War II improved the research of the EM absorbers, with interest in wave absorbers for the military. Germany used it as an absorber for radar camouflage, and in the United States was used to improve radar performance by reducing interfering reflections from nearby objects. In the United States, O. Halpern created a project at the MIT Radiation Laboratory to bring a wave absorber coating, and they have developed the Halpern AntiRadar Paint (HARP) [4]. The produced HARP absorber uses artificial dielectric material with a thickness of about 0.6 mm, offering 15-20 dB reflection reduction at resonance. In 1953, Neher et al. [4] developed the pyramidal wave design absorber with the same material, and high accuracy measures became a reality in experiments such as the measurement of antenna patterns in an anechoic chamber.

2.8.2 Absorbing Materials

Absorbers can be divided into three families: electrically, magnetically, and hybrid. Electrically losses are produced with foam, impregnated, or coated with electrically lossy materials, making the material more suited for high-frequency. This absorber family is widely used to do antenna and RCS measurements. Magnetic losses are a smaller family than the electrical ones, made of ferrite materials shaped as thin layers, or tile or plastics, loaded with ferrite powders, perfect for low-frequency measurements. Ferrites, commonly used in the manufacturing of microwave components such as isolators and circulators, are complex materials that are very frequency-dependent. The hybrid absorbers shared both previous family characteristics, providing the low-frequency performance of the magnetic loss materials and the high-frequency performance of the electrical loss materials. [6].

2.8.2.A Ferrite Tiles

The ferrite tiles, as illustrated in Figure 2.13, are used in the frequency range from 30 MHz to 1 GHz, which reveals high performance in low frequency, and is also space-efficient compared to foam in the same frequency range because they are too heavy and cannot be used for high frequencies. Ferrite tiles are inherently immune to fire, humidity, and chemicals, providing a reliable and compact solution to reduce plane wave reflections in shielded chambers.

Figure 2.13: Exemplar of a Ferrite tile, adapted from [21].

2.8.2.B Hybrid Absorber

Hybrid absorber, as illustrated in Figure 2.14, is the result of combining ferrite tiles and microwave pyramidal foam, with a frequency range from 30 MHz to 18 GHz, and the main requirement of this material is the foam must have a good impedance match with the ferrite. It has a pyramidal shape with more dielectric materials included in the foam. The secret of this absorber type at lower frequencies is to gradually increase dielectric-loaded materials enhancing energy dissipation, inducing high losses at low frequencies [22].

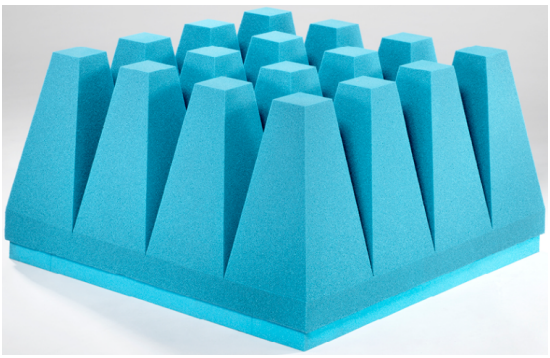

Figure 2.14: Exemplar of a Hybrid Absorber, adapted from [23].

2.8.2.C Microwave Absorber

The microwave absorber, the most used absorber material, has a usable frequency range from 100 MHz to 18 GHz, although, at low frequencies, its performance is lower than the ferrite tiles. It is often solid urethane foam and can be applied indoors or outdoors. For indoors, it is used inside AC covering walls, ground, and ceiling. For outdoor it is used in the specular region. This absorber is light and easier to hold on the chamber walls but also fragile. The weak points are the interaction with fire, humidity, and temperature. There are two main types of microwave absorbers, the pyramidal, illustrated in Figure 2.15, and the wedge-shaped, shown in Figure 2.16.

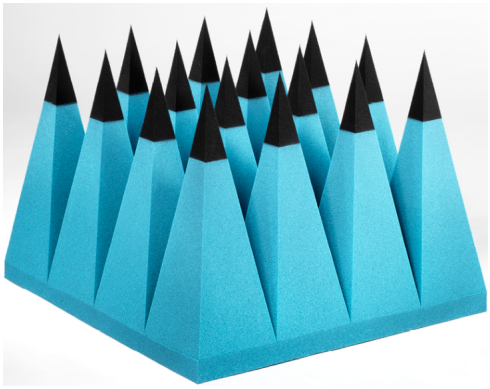

Figure 2.15: Exemplar of a Microwave Pyramidal Absorber, adapted from [23].

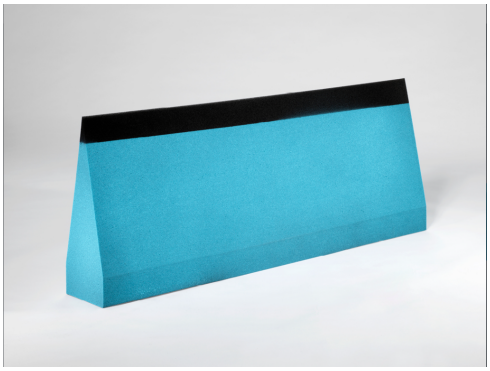

Figure 2.16: Exemplar of a Wedge-shaped Absorber, adapted from [23].

In [24], Nornikman et al. presented a performance simulation of pyramidal and wedge microwave absorbers designed to operate effectively in microwave frequencies from 1-10 GHz. They perform simulations to use a fusion of carbon-based material with different features and coating thickness to improve their performance and cost savings. They have concluded that the normally truncated pyramidal absorber showed the best performance, and the coating of half the absorber height resulted in the best performance in terms of signal absorption.

2.8.3 Radio Wave Absorber Characterization

Radio Wave absorbers are essential for AC to work with high-performance design and materials, planned carefully to provide the best absorption of radio waves entering or exiting the chamber. The performance of each absorber is determined by the reflection coefficient Γ, which is the relation between the magnitude of reflected E_r and incident E_i electric-fields of plane waves given by:

$$\Gamma = \left(\frac{E_r}{E_i}\right) \tag{2.28}$$

The absorber performance can also be described by return loss RL in decibels, given by:

$$RL_{[dB]} = -20\log(\Gamma) \tag{2.29}$$

The higher the value of $RL_{[dB]}$, the better the absorber performance. It is important to minimize reflections from absorbing materials because they can represent constructive or destructive interference at the receiving antenna, typically the AUT.

2.9 Anechoic Chamber State of the Art

This section presents a set of papers that include ACs development choices such as size, design, and absorber properties. Furthermore, it will be described the results and the improvements done on this topic.

2.9.1 Rectangular Chambers

A small rectangular AC is described in [25] with a size of 2.25 m (W) x 1.20 m (H) x 1.20 m (L) and frequencies between 18 GHz to 30 GHz. It is a stand-alone metal box, shielded using a 1.2 mm thick aluminum sheet and supported by an external wooden skeletal frame to provide mechanical rigidity. The chamber walls have two types of absorbers, the back wall, central sections, roof, and floor lined with 150 mm depth pyramidal type, and the remainder lined with 80 mm depth profiled type material. This chamber performs a reflectivity level better than -52 dB for the frequencies mentioned.

In [26], the authors have proposed a low-cost anechoic chamber to reduce production costs. The proposed structure was a rectangular chamber with 1.6 m (W) x 1.1 m (H) x 1.1 m (L) covered with pyramidal absorbers and shielded with zinc to avoid any external microwave signal. In this scenario, the pyramidal absorber was prepared for a frequency range from 3 GHz to 15 GHz, although the test was only for 10 GHz. The authors also have designed three polystyrene absorber prototypes to compare with the commercial absorber. Prototype 1 was 20 cm in height, prototype 2 was 15 cm, and prototype

3 was the absorber with less carbon. After the measurements, the absorption rate of prototype 1 was 2.5 dB lower than the commercial one, with an absorption rate of 39.8 dB against 42.3 dB. Prototype 3, with less carbon, only achieved an absorption rate of 23.5 dB.

In [27], the authors presented a low-cost anechoic chamber with a low-cost absorber using composite materials to reduce costs. The proposed structure was a rectangular chamber with 1.2 m (W) x 0.8 m (H) x 0.8 m (L) covered with pyramidal absorbers with 0.2 m x 0.2 m x 0.2 m and shielded using plywood. The frequencies used were 500 MHz and 2 GHz using a monopole antenna. For 2 GHz frequency with no absorber, the average power received was -42.5 dBm, and an absorber assembled inside the chamber was -105 dBm. The average absorption rate of the low-cost absorbers with carbon was 42.2 dB, and without carbon, 33.2 dB. The average absorption rate of the commercial absorber was 50 dB, reaching a performance 16% better than the best low-cost absorber solution. Finally, the low-cost portable chamber performs absorptions rates of 62.5 dB for 2 GHz and 40.8 dB for 500 MHz.

The ”Two-Level GTD” method has been presented in [28] to decrease the reflectivity and enhance overall performance for anechoic chambers operating at frequencies above 1 GHz, where the typical dimensions of the side-walls are usually more than 30λ. It contains the shaping of the side walls of an anechoic chamber with an application of a ”fish-bone” absorber layout designed and established on GTD principles. This method was also applied in [29] to improve reflectivity in an anechoic chamber with external dimensions as small as 18’(H) x 18’(W) x 33’(L) operating from a low frequency of 100 MHz.

In [30], Chung Liu et al. proposed an innovative design of AC to provide EM radiation measurement in the test zone for low frequency range. For this range, the conventional design needs a long taper chamber or a large rectangular size with 12 m (W) x 5 m (H) x 5 m (L) dimensions. The result size of the chamber was 6.5 m (W) x 3.86 m (H) x 3.85 m (L), providing superior uniformity in the quiet zone at the VHF band compared with the conventional rectangular design with a bigger size.

In [31], the authors designed an electrically-large anechoic chamber for the millimeter-wave band. The authors have used the Ansys Savant software to perform simulations using physical optics coupled with a uniform theory of diffraction (PO/UTD) and an open waveguide probe method to obtain the absorber characterization parameters for this band. The final design results in a chamber with a size of 1.2 m (W) x 0.6 m (H) x 0.6 m (L), achieving the most significant QZ with 30 mm x 30 mm x 50 mm size using a horn antenna with 25 dBi for a frequency 75 GHz.

In [32], Suganthi et al. designed and built a rectangular AC with 7 m x 4 m x 3 m dimensions, set up for the 100 MHz to 40 GHz frequency range. However, the test range was shortened for the 800 MHz to 40 GHz interval due to antenna issues. After some validations and tests, the authors achieved overall shielding effectiveness of -80 dB and reflectivity of -40 dB in one cubic meter area at the AUT region, 5.5 meters away from the transmitter. The AUT is above a rotational motorized system that can change the azimuth angle in 9º intervals to plot the radiation pattern accurately.

An innovative design concept of the Passive Intermodulation (PIM) test chamber is presented in [33] by controlling the PIM source level of the AC instead of increasing the size of the chamber. The authors developed an absorbing material and shielding enclosure structure with extremely low PIM to implement this concept. Two PIM test chambers were built, chamber A with innovative design and external dimensions of 3.96 m (L) x 2.62 m (W) x 2.6 m (H) and chamber B with standard design and external dimensions of 7 m (L) x 4 m (W) x 3.5 m (H). The results show that the PIM generated at the chamber with the standard design has more than 10 dBc measured third-order PIM than the new design.

A mini chamber is presented in [34] and was designed for a frequency range, beginning at 1 GHz to 5 GHz. The authors used an old refrigerator whose inside dimension is 24'(L) x 14.5'(W) x 19' (H) to provide the necessary shielding and enclosure. They have performed four consecutive tests to ensure the functionality of the chamber, splitting it into two conclusions. The first was a test of absorption and enclosure, performing S_{12} and S_{21} measurements using two GSM antennas at 2.5 GHz, one placed inside and the other outside the chamber. For the S_{12} measure, the received signal was -88.35 dB, and S_{21} was -83.651 dB, concluding that the energy does not pass the chamber walls. The second conclusion was measuring the S_{11} parameter, and the antenna showed minimum reflection at its resonant frequency.

2.9.2 Tapered Chambers

For the low-frequency range testing, Emerson invented the tapered design in 1967 after filing the patent in 1964 [18]. The design basics are from the GO, antenna theory, and an array of source theory viewpoints. While explaining the design by the antenna theory, the tapered design takes the large antenna wall covered with lossy absorbers.

Vicente Rodriguez presented, in 2012 [35], a chamber where the conical shape of the launch is continued through the entire length of the tapered chamber. The regular tapered chambers are constructed using a square-based pyramidal-shaped taper. The taper is then shaped into an octagon and finally transformed into a cylindrical launch section. This new full cylindrical design results in the free space Voltage Standing Wave Ratio (VSWR) test over a 1.5 m diameter QZ at different frequencies in the range from 200 MHz to 18 GHz with QZ reflectivity levels that exceed -30 dB. This chamber showed better results than the standard approach in terms of better illumination wavefront and better QZ levels even at frequencies above 2 GHz. The resulting chamber, which uses the conical taper, has its QZ scanned using the free space VSWR test.

In 2015, Zhang et al. [36] made compact and flexible embroidered spiral antennas that can be used for wearable applications. The antenna has been measured on a Specific Anthropomorphic Mannequin (SAM) phantom and a real human. The measurement results show that the SAM phantom emulates the dielectric properties of the human body in a wide frequency band from 0.3 to 3 GHz. The far-field

on-body performance of the antenna has been measured by placing the antenna on the SAM phantom in a tapered AC. The authors have used this tapered chamber to compare antenna measurement parameters as S_{11} and radiation pattern. S_{11} represents how much power is reflected from the antenna, and hence is known as the reflection coefficient [37].

A cone-shaped tapered AC approach is presented in [38], considering a mathematical model of a cone-shaped tapered AC with a cylindrical part. The chamber walls were initially considered perfectly conductive and calculated the distribution of the EM field strength. The author compared the behavior of the electric field when the angle of the aperture of the cone changes.

Two types of tapered AC, conical and pyramidal, often used for measurements at low frequencies, were analyzed by mathematical simulation in [39]. The chamber has 10 m in the rectangular part, the pyramidal section is 15 m in length, and the conical version with 16.93 m. The QZ of both chambers at 250 MHz were approximately the same (3.2 m x 3.2 m for the conical design and 3.4 m x 3.0 m for the pyramidal design). For 800 MHz, the sizes of the QZ decrease for both chambers (1.8 m x 1.8 m in the conical and 1.7 m x 1.7 m for the pyramidal). After these lower results, the authors used a dielectric lens to perform a correction. After the lens correction, the QZ increased to 3.3 m x 3.3 m in the conical chamber and 2.4 m x 2.6 m in the pyramidal chamber.

In [40], the performance of the quiet zone of a tapered range is analyzed from 100 MHz to 1 GHz. The chamber under analysis has a rectangular section of 4.9 m by 4.9 m by 4.9 m, with a tapered section having a subtended angle of 27.8 degrees and a length of 9.3 m per section. The absorber treatment is a 1.82 m pyramidal absorber on the end wall and a 45 cm pyramidal absorber on the specular areas, with the balance of the interior surfaces treated with a 20 cm tall wedge absorber. The analysis indicates that based on the phase distribution, the tapered chamber is a far-field measurement and that the performance depends on the absorber surrounding the range antenna. The chamber QZ is a 1.82 m sphere located 3.35 m from the end wall.

2.9.3 Alternative Chamber Structures

A multipurpose anechoic chamber is presented in [41] to operate over a wide frequency range, from 30 MHz to 18 GHz. The chamber geometry is asymmetrical due to a combination of rectangular and tapered volumes. The chamber size is about 64 ft x 32 ft x 24 ft high. A plane-boundary model has been used to model the walls and ceiling, covered with microwave absorbers. The authors used a beam-tracing technique to predict normalized site attenuation. It achieved the desired wideband performance using lower-cost wave absorbers and a unique asymmetrically shaped geometry. The ease of construction and lining with the absorber is also necessary features of the design.

There are other chamber shapes as a fully metalized ellipsoid AC designed to guide the EM wave to the spherical absorbers [42]. This shape has based on the two-focus theory of the ellipse. The source

antenna is at one focus of the ellipse, and the spherical absorber is at the other. All the reflected waves from the metalized chamber reach the focus where the spherical absorbers are kept and are absorbed, providing an excellent QZ, according to the ray theory. To decrease the back-radiation, the side where the source antenna is cut. The source antenna, phase center, should be placed at the focus of the ellipse. This design can decrease the overall use of the absorbers. However, broadband absorbers can be used for a range of frequencies. Taking the idea from the previous design, the parabolic metalized AC in [43] can give great QZ size inside it, based on the two-focus theory also, with source antenna stands placed at one of the sides and the absorbers at the opposite side.

In the case of size constraints, the Compact Antenna Test Range (CATR) is the chosen design. Here, a large parabolic dish reflector is used to generate the plane wave from the spherical wave from the range antenna, i.e., feed. It has a simple operational principle initially proposed by the author of [44]. However, the construction design should be done carefully to decrease the diffraction field from the edges. The process is to serrate or roll the edges to reduce the ripple fields in the QZ. In [44], the authors made the three types of edge treatment. The top edges were rolled, the two sides serrated, and the absorbers placed at the bottom edge.

A new design of CATR is reported in [45]. A diamond-shaped reflector is used in the corners parallel to the side walls. The reflected fields from the corners are 6-10 dB lower than at the edges. The corner field will illuminate the side walls. Thus lower scattering is observed. Also, the edge fields will die down as they reach the corners. This design helps in giving superior QZ.

For testing the MIMO antenna, the far-field multi-probe AC is required. The compact range is not suitable for the MIMO as it only generates one pseudo-plane wave. However, the problem can be mitigated if the feed position changes, giving multiple plane waves. The problem with changing the location of the feed is an increase in the phase and amplitude tapers in the QZ. [46] shows the use of parabolic-toroid reflector in the CATR. The amplitude taper and ripple for azimuth and elevation angle (in the $\pm 15^{\circ}$) are below the prescribed limit of 1 dB and ± 0.5 dB, respectively. Nevertheless, the phase ripple of more than the prescribed limit of $\pm 5^{\circ}$ is observed at other elevations.

A CATR shown in [47], designed to have a shorter focal length reflector. The reflector is a diagonal feed placed near the reflector, consequently decreasing the overall size of the chamber by 50%. This placement causes less scattering as the feed is not placed in the plane wave view. Also, the positioner system is far from the feed system. Thus the mechanical movement of the two systems is not restrained. A mini CATR, designed by ORBIT/FR. Inc for the automotive radars having small antenna apertures up to 50 cm from the frequency range of 4 to 110 GHz is described in [48]. The test range is used for onsite and off-site testing due to rolling wheels. The maximum quiet zone available is 50 x 50 cm^2.

3

Characterization of the Absorbent Material

Contents

This chapter describes the absorber material characterization, starting with the simulations, using the EM software CST Microwave Studio, of different structures to understand why pyramidal design is the best to use as an absorber. It also presents a novel absorber and a novel MM design to improve absorbent performance based on the pyramidal absorber structure. Lastly, it is presented the report of the laboratory tests on two absorber materials made inside an AC.

3.1 Absorbent Material Analysis

The goal of a good absorber material is to transform the energy of an incident wave into a different kind of energy with the lowest reflections possible. In [4], Emerson describes the use of broadband material for reducing the radar signature, comprised of layers of plastic and a resistive sheet. The resistance of these sheets decreased at an exponential rate toward the back surface of the material. The goal of the resistance taper was to allow for a gradual penetration of the wave into the absorbent material avoiding undesired reflections. The gradual penetration of the wave reduces the reflection coefficient eq. (2.28), granting a better absorption.

Hence, the absorptivity A can be calculated using the equation 3.1 [49], [50]:

$$A = 1 - |S_{11}|^2 - |S_{21}|^2 \tag{3.1}$$

where S_{11} is the reflection coefficient and S_{21} is the transmission coefficient, respectively.

Parameter $|S_{11}|^2$ and $|S_{21}|^2$ can be unfolded as [49], [50]:

$$|S_{11}|^2 = |\Gamma_{xi}|^2 + |\Gamma_{yi}|^2 \tag{3.2}$$

$$|S_{21}|^2 = |T_{xi}|^2 + |T_{yi}|^2 \tag{3.3}$$

where x and y indicate the axis along which the reflection or transmission coefficient is observed, respectively, and the second parameter, i, represents the direction of the incident electric field. When the second parameter i becomes x, the parameters $|S_{11}|^2$ and $|S_{21}|^2$ indicate the ratios of reflected power and transmitted power respectively. As opposed to those of reflected and transmitted fields. Likewise, the absorptivity A is an absorption ratio of incident power [49]. A metal plate is placed at the bottom of the absorber base to reach zero transmission coefficient. Hence, the absorptivity is maximum if reflectivity is minimum or ideally zero.

3.1.1 Absorbent Material Design Analysis

An important question is why the pyramid design is the most suitable. Following the theory in section 3.1, cutting the material into pyramidal shapes produces a similar result as these resistive layers with lower costs. The pyramidal shape form allows maximum penetration of the incident wave energy at the surface and, thus, maximum absorption at the lossy base by gradually tapering the intrinsic impedance of the structure from the incident media to the base material [51].

As the wave hits the boundary between free space and absorber material, some will be transmitted, and some will reflect. The reflection coefficient can be written as [6]:

$$\Gamma = \left(\frac{\eta_1 - \eta_0}{\eta_1 + \eta_0} \right) \tag{3.4}$$

where η_0 is the impedance of free space ($\eta_0 = 120\pi\ \Omega$), and η_1 is the wave impedance inside the absorber. The impedance inside the absorber (η_1) is given by the equation 3.5 [6]:

$$\eta_1 = \sqrt{\frac{j\omega\mu}{\sigma + j\omega\epsilon'}} \tag{3.5}$$

As Figure 3.1 presents, as the incident wave penetrates the material, the wave impedance shifts from free space to an effective wave impedance.

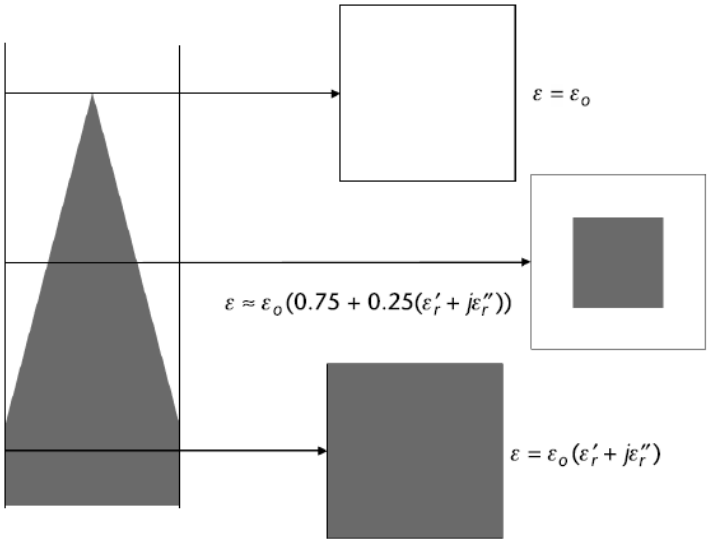

Figure 3.1: Reasoning behind the pyramidal shape as a method for obtaining an impedance taper (adapted from [6]).

As the wave penetrates the material, the correspondent impedance is a weighted average of the permittivity of the material and the permittivity of the surrounding free space until reaching the base of the pyramidal absorber.

The CST software can demonstrate the theory by testing different formats and comparing the S_{11} value. For a fair comparison, it is essential to use the exact dimensions and the same material. The designs chosen in this scenario to comprehend why the pyramids are suitable for absorbers are a rectangular prism, a pyramid, and a cylinder, as shown in Figure 3.2.

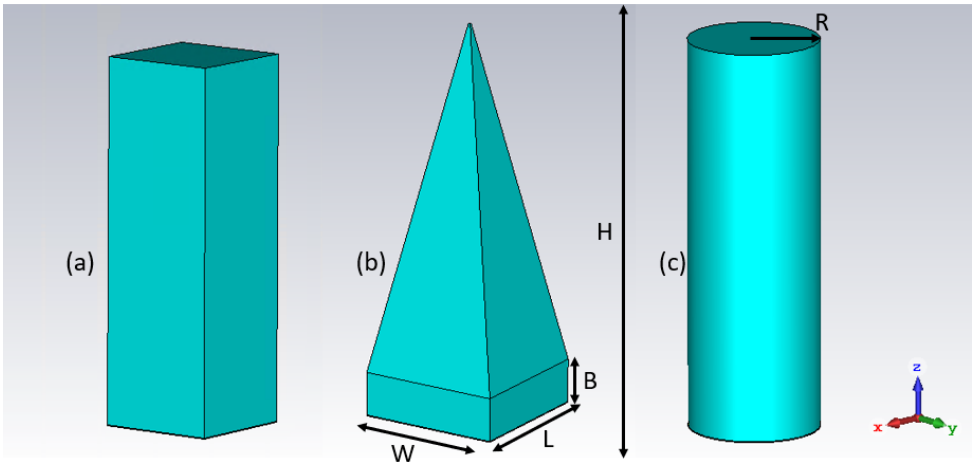

Figure 3.2: Rectangular Prism absorber (a), regular pyramid absorber (b), and a cylinder absorber (c).

The CST simulations use the unit cell concept for each absorber design. Each unit cell is excited using floquet ports providing electric and magnetic fields along the x-axis and y-axis and propagation vector along the z-axis, from Zmax to Zmin. All tested designs have the same material composition and sizes as described in Table 3.1.

Table 3.1: Absorber Design Comparison - Size Parameters.

Figure	W(mm)	L(mm)	B(mm)	H(mm)	R(mm)
(a)	15	15	N.A.	45	N.A.
(b)	15	15	5	45	N.A.
(c)	N.A.	N.A.	N.A.	45	7.5

A metal plate is placed at the bottom of each absorber to eliminate the transmission component, simplifying the absorption equation that only depends on the material's reflectivity. The absorber dimensions match a scaled size of 1:10 to reduce complexity and simulation time. The range frequency used is from 1 to 12 GHz. The first approach defines a normal incidence angle as $\theta = 0°$, and the second approach represents an oblique incidence angle $\theta = 45°$.

Figure 3.3(a) shows the simulation result for the normal incidence angle. The design with the better performance is the standard pyramid design. The cylinder and the rectangular prism designs can only achieve a S_{11} of -8 dB at 12 GHz. Contrarily, the pyramid design can reach almost -70 dB of S_{11} for 6.5 GHz and -30 dB to -50 dB of S_{11} in practically all the test ranges. Figure 3.3(b) shows the simulation result for a incidence angle $\theta = 45°$. In this simulation, the results are similar, with a reduced S_{11} for all

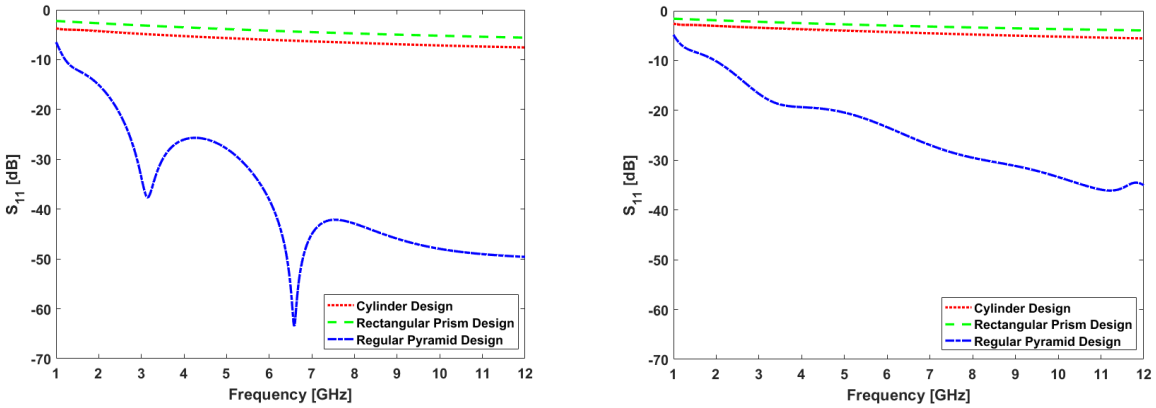

(a) Normal incidence angle.

(b) Incidence angle $\theta = 45^{\circ}$.

Figure 3.3: S_{11} for different incidence angles.

designs. Still, the pyramid design has the best absorption performance compared with the cylinder and the rectangular prism. While the incidence angle increase, it is expected that the difference of the S_{11} between the different designs will be even less, and the absolute value lower.

3.2 Novel Absorber Structure

The absorber industry has improved its production process, as many absorber types have emerged in recent years. As tested before in this dissertation, the pyramid design has higher absorption performance than others, being the most used. Beyond the conventional pyramid, other similar absorbers are produced with specific ranges or high thermal resistance improvements.

ComTest is one of many manufacturers of absorber material. The ComTest MT45 absorber, as shown in Figure 3.4, is a polystyrene absorber widely used for AC wall covering. This material is well known for its durability compared with polyurethane foam materials and uses in diverse antenna measurement applications. The frequency range of this material is from 300 MHz to 50 GHz with a S_{11} better than -20 dB. Furthermore, this chapter also presents this material structure to compare the design performance with other design materials as the regular pyramid. At the end of this chapter, a laboratory test will be described inside an AC at Instituto de Telecomunicações (IT) facilities that use this ComTest material to cover the walls.

The objective is to compare the S_{11} performance of a novel absorber structure with the ComTest design and the standard pyramidal absorber for the frequency range of 1 to 12 GHz by simulation for both the elevation and azimuth plane. Typically the absorber manufacturer does not mention the performance of the absorbers for more than the incident angle.

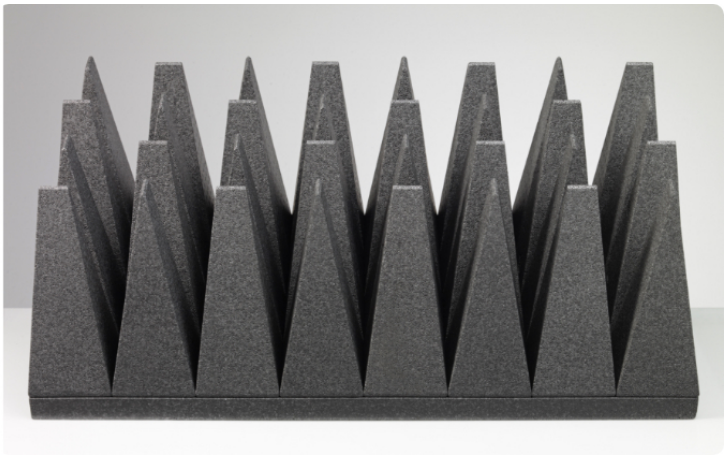

Figure 3.4: ComTest MT45 absorber design.

The top part of the novel absorber contains four pyramids. Each pyramid cell has a perpendicular side to the base, as the pyramid appears sliced in half. Using more cells allows a perfect join between sliced pyramids, creating a design similar to the pyramidal absorber with higher performance. Figure 3.5 illustrates the ComTest design, the novel design, and the traditional pyramid design.

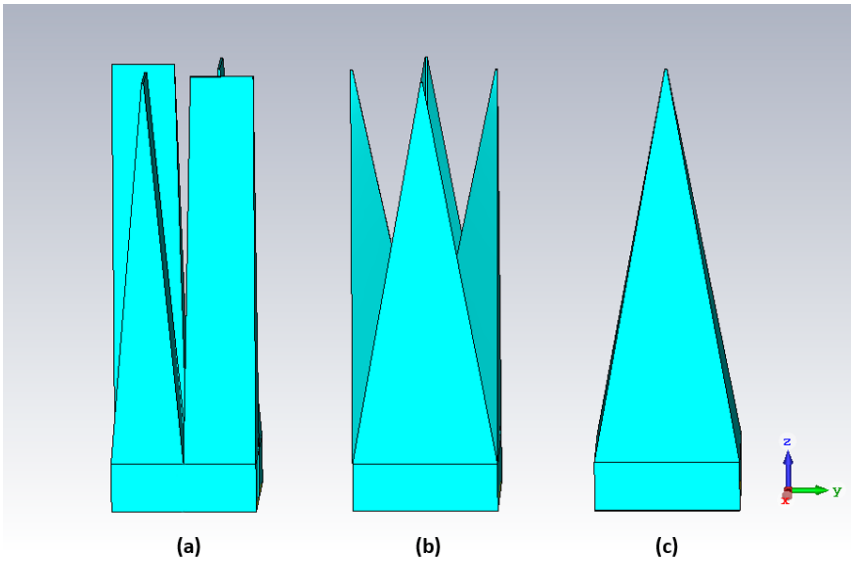

Figure 3.5: ComTest Design (a), Novel Design (b), and Regular Pyramid (c).

The size parameters follow the regular pyramid parameters described in Table 3.1. A comprehensive way of understanding the improvement provided by this novel design is to compare its performance with the ComTest MT45 and the traditional pyramid designs. Figure 3.6 shows the performance of the three absorbers differing θ from $0°$ to $75°$.

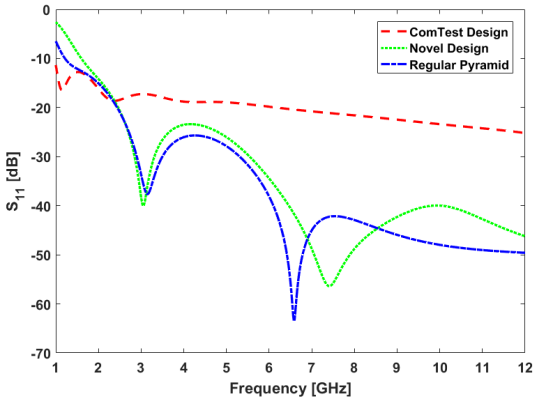

(a) Normal incidence angle.

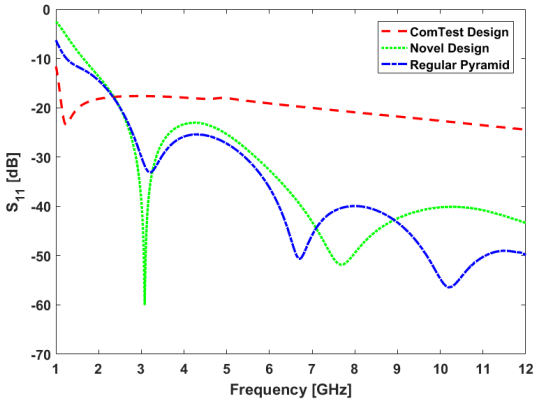

(b) Incidence angle $\theta = 15^{\circ}$.

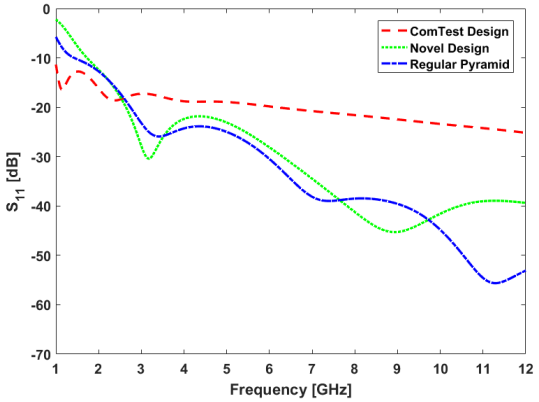

(c) Incidence angle $\theta = 30^{\circ}$.

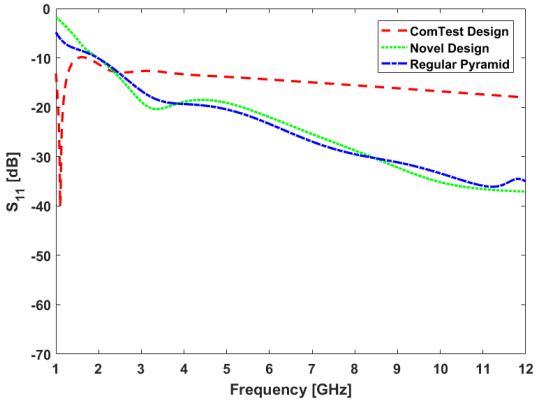

(d) Incidence angle $\theta = 45^{\circ}$.

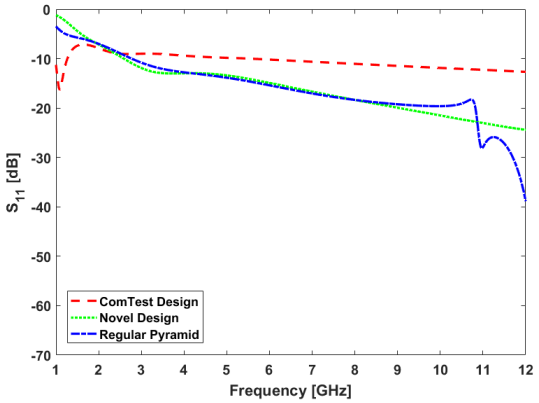

(e) Incidence angle $\theta = 60^{\circ}$.

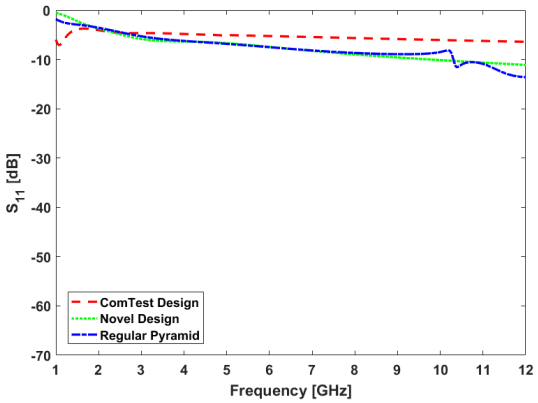

(f) Incidence angle $\theta = 75^{\circ}$.

Figure 3.6: S_{11} for different incidence angles.

In the normal incidence graphic, Figure 3.6(a), the ComTest design performs better until 1.5 GHz compared with the others. After 2 GHz, this design has the worst S_{11} value of the three absorbers, with the best S_{11} value around the -20 dB. The novel design follows the pyramid performance design until 6 GHz, with better performance only between 7 and 8 GHz.

In Figure 3.6(b) and Figure 3.6(c), the behavior is similar with an increased bandwidth advantage for the ComTest design that can stand with higher performance until 2.5 GHz. The novel absorber performance follows the regular pyramid until 7 GHz.

Figure 3.6(d) shows the best performance of the ComTest design for low frequency. The novel and ComTest designs have now reduced the S_{11} value by 20 dB compared with the normal incidence angle. However, the performance is still below the -20 dB in almost all ranges. Figure 3.6(e) and Figure 3.6(f) show the effect of the high incidence angles on the absorber with substantial performance reductions. For the $\theta = 60°$, the regular pyramid performs better above 10 GHz.

The novel design's performance follows the standard pyramid's performance until the high-frequency range. For lower frequencies, the performance is better in some ranges. The solution involves some improvements on the absorber to provide higher absorption for the high-frequency range.

3.2.1 Metamaterial

A MM unit cell was developed for the bottom of this novel design to improve the absorption characteristics and reduce the height of the absorber. Due to their flexible design, MMs acquired huge attention in microwave absorbers [50]. MMs can create independent customized electric and magnetic responses to incident radiation. They provide geometrically scalable raising operability over a substantial amount of EM ranges. A MM can be impedance-matched to free space, minimizing reflectivity [52]. The goal is to achieve better S_{11} performance for both vertical and horizontal planes.

Lately, resistive films with high accuracy, uncomplicated fabrication, and low cost have attracted a lot of attention, among which a material designated Indium Tin Oxide (ITO) has excellent optical transparency and electric conductance. MM absorbers, with their unique physical properties established on ITO films, can achieve high optical transmittance and broadband microwave absorption [52].

A MM unit cell is proposed to reduce the absorber base thickness from 5 mm to 1.03 mm and improve the absorption of the novel absorber design. The proposed structure is presented in Figure 3.7, and the sizing details are in Table 3.2.

Table 3.2: Unit Cell Parameters.

W(mm)	L(mm)	Thickness(mm)	E1(mm)	E2(mm)	E3(mm)
15	15	1.03	0.85	1.42	0.93

This proposed structure with different layers of different materials and thicknesses is illustrated in

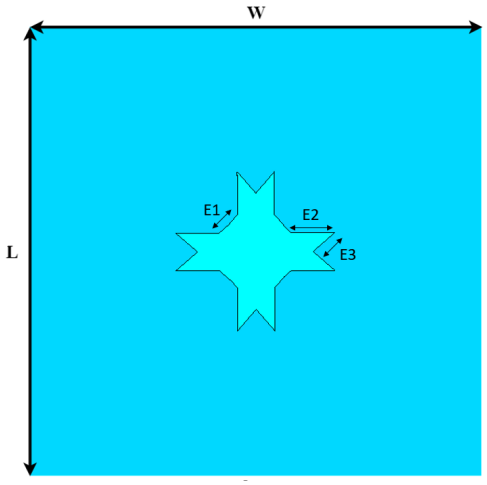

Figure 3.7: Top view of the proposed unit cell MM.

Figure 3.8. The unit cell presented consists of a Polystyrene base layer covered with Polyethylene terephthalate (PET) and ITO substrate, having the sheet resistance (R_s) of 400 Ω/sq. The reason for using this type of metamaterial was the excellent results achieved in [53] with a similar structure but with a different cut pattern on the top layer. The copper plate layer is placed at the bottom of the MM absorber to remove wave transmission.

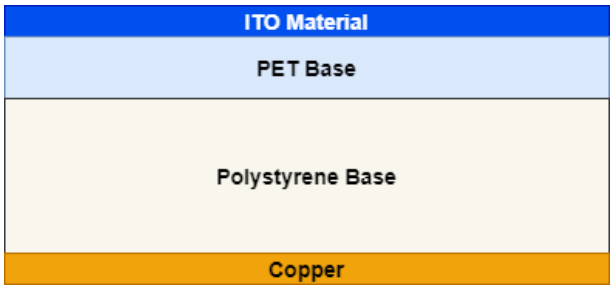

Figure 3.8: Schematic side view of the proposed MM unit cell composition.

The pattern is based on a Portuguese medal designated ”Grã Cruz”. This design is a four-fold symmetrical pattern structure. This structure breaks the four-fold rotational symmetry of meta-atoms and enables strong coupling between different polarization states. This coupling makes conceivable a practically complete cross-polarization conversion upon reflection of polarized waves from the metamaterial surface [54]. This structure made up of ITO+PET is temperature stable till $120°C$

Simulating the structure fields makes it possible to witness the four-fold rotation symmetry. The frequencies used for the simulation were 1 GHz and 3 GHz, as shown in Figure 3.9.

Figure 3.9(a) and Figure 3.9(b) illustrates an electric field around the structure pattern. There is an

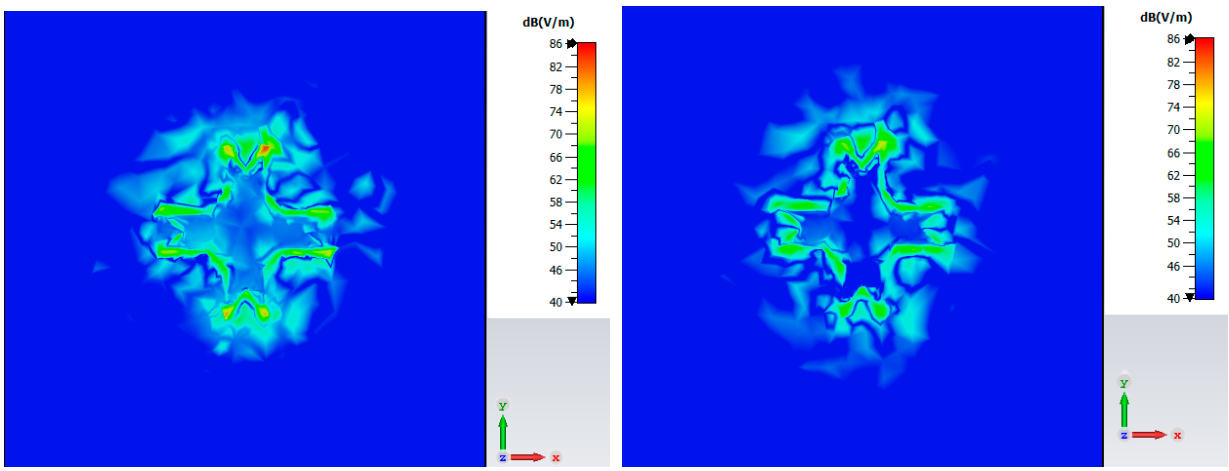

(a) MM unit cell E-Field contour analysis for f=1 GHz.

(b) MM unit cell E-Field contour analysis for f=3 GHz.

Figure 3.9: MM unit cell E-Field contour analysis for 1 GHz and 3 GHz

electric charge loop feeding an electric dipole resonance. The strong electric field at the corners of the etched pattern and the dielectric material in the middle creates the capacitance effect. An electric dipole moment is created due to the charge accumulation at the corners. Due to the anti-parallel surface current on the front and back sides, the current loop is formed, and a magnetic dipole moment is created. This phenomenon can also be seen using a surface current analysis using arrows that shows the current flow direction, illustrated in Figure 3.10 and Figure 3.11.

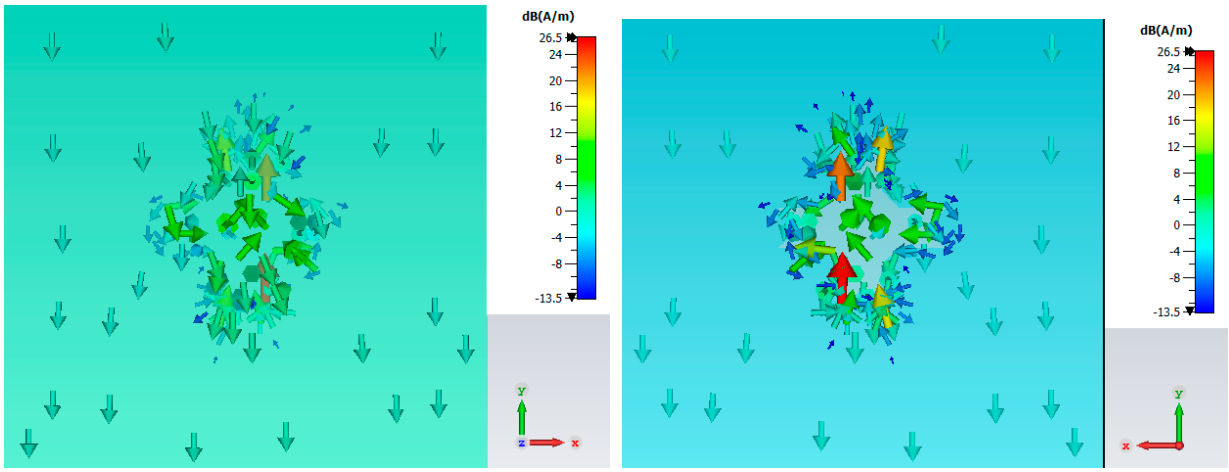

(a) MM unit cell front side surface current analysis for f=1 GHz.

(b) MM unit cell back side surface current analysis for f=1 GHz.

Figure 3.10: MM unit cell front and back side surface current analysis for 1 GHz.

In this analysis, Figure 3.10(a) and Figure 3.11(a) are representing the front side MM unit cells

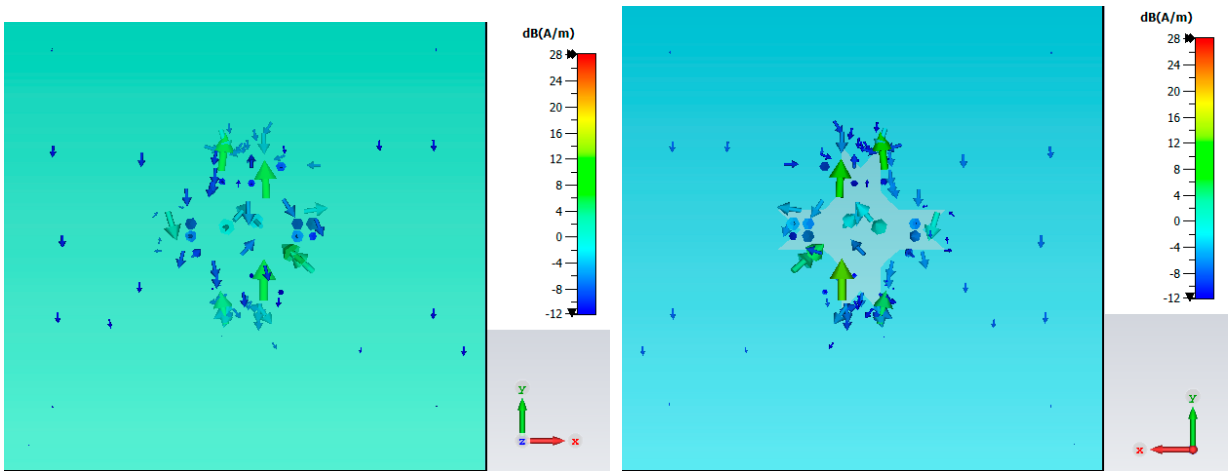

(a) MM unit cell front side surface current analysis for f=3 GHz.

(b) MM unit cell back side surface current analysis for f=3 GHz.

Figure 3.11: MM unit cell front and back side surface current analysis for 3 GHz.

showing the current flowing in one direction, and the back side Figure 3.10(b) and Figure 3.11(b) of MM unit cells flow in the opposite direction. Creating a current loop, thus creating a magnetic dipole resonance.

3.2.2 Novel Design with MM Performance Analysis

This section presents the simulation results between a conventional pyramid absorber, a ComTest MT45 absorber, and a proposed novel design absorber with and without MM, as illustrated in Figure 3.12.

The simulations used a frequency domain solver to perform the floquet analysis, and the absorber material used for all designs is the CST preloaded ECCOSORB QR-13AF [55]. The absorber dimension characteristics are described in Table 3.3.

Table 3.3: Absorber Size Parameters.

Figure	W(mm)	L(mm)	B(mm)	H(mm)
(a) , (b) and (d)	15	15	5	45
(c)	15	15	1,03	41

The base width of the absorber structures (period of absorber array) is 15 mm, and the height is 45 mm for (a),(b), and (d), with a base thickness of 5 mm. These absorber dimensions match a scaled size of 1:10 to reduce complexity and the simulation time. The range of frequency used is from 1 to 12 GHz. Figure 3.13 shows the S_{11} simulation results.

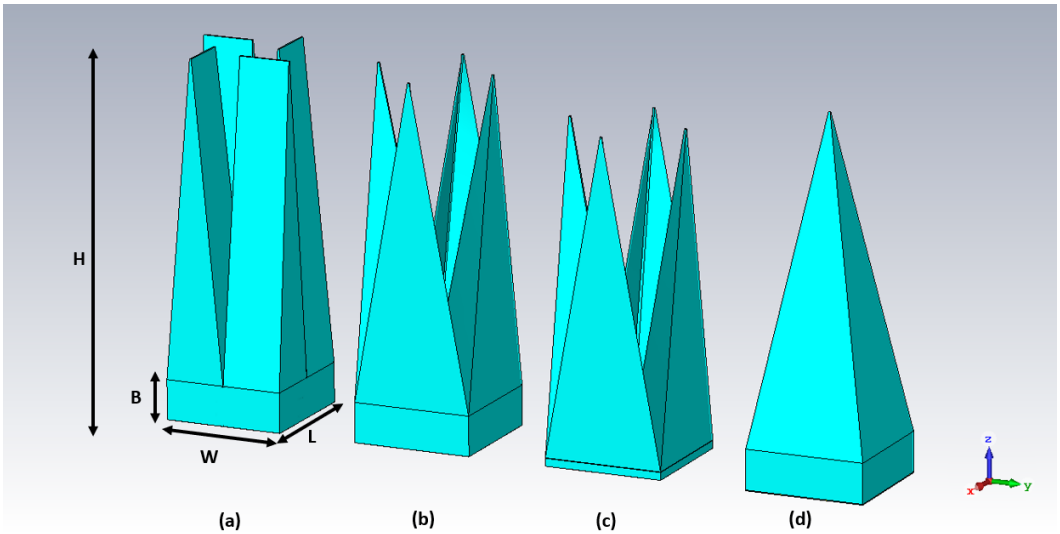

Figure 3.12: ComTest design absorber (a), Novel design without MM absorber (b), Novel Design with MM absorber (c), and Regular Pyramid absorber.

From Figure 3.13(a) until 10 GHz, the novel design with MM maintained almost the same S_{11} as the conventional pyramidal absorber. Although for higher frequencies, the performance of the proposed novel structure starts to give some performance improvement, thus proving that the design is suitable for higher frequencies. The S_{11} of -55 dB is observed at 5.5 GHz for the proposed structure. The model's S_{11} value is greater than the traditional pyramidal absorber value by more than 10 dB for frequencies over 10 GHz. The performance of this novel design is expected to improve even more with increased frequency.

Figure 3.13(b) shows an improvement in the performance of the novel absorber with the MM compared with other designs. From 7 GHz, this design has a higher performance than the regular pyramid and the novel absorber without MM.

From Figure 3.13(d), the proposed structure shows the same performance as the conventional regular pyramidal until 5 GHz, with a one-off advantage at 2.5 GHz. For higher frequencies, an increased performance of 7 dB is observed compared with the traditional pyramid. Hence, there is no performance degradation even with the broad angle of incidence. This simulation proves that the proposed structure is stable even for wide incident angles with reduced base thickness, which increases the free space inside the chamber and reduces the weight.

As illustrated in Figure 3.13(e) and Figure 3.13(f), the performance of the absorber suffers a performance decline for angles of incidence above $\theta = 40°$. The ComTest design was again the worst absorber design of all the tested models. Except for the lower frequencies, this absorber's S_{11} never surpasses the -20 dB in all frequency ranges above 2 GHz.

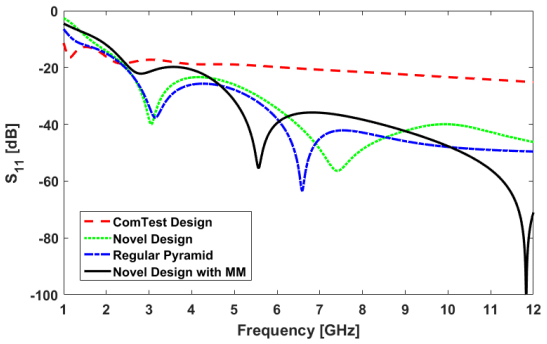

(a) Normal incidence angle.

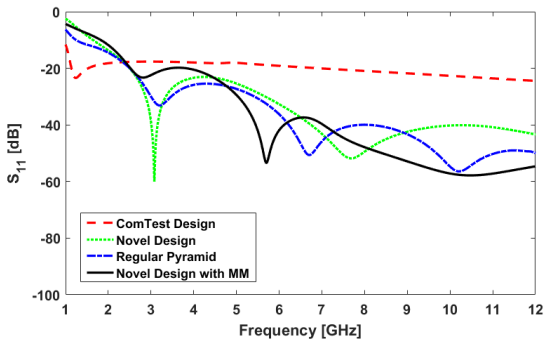

(b) Incidence angle $\theta = 15^{\circ}$.

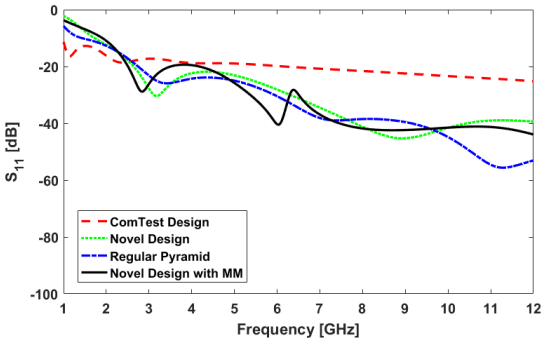

(c) Incidence angle $\theta = 30^{\circ}$.

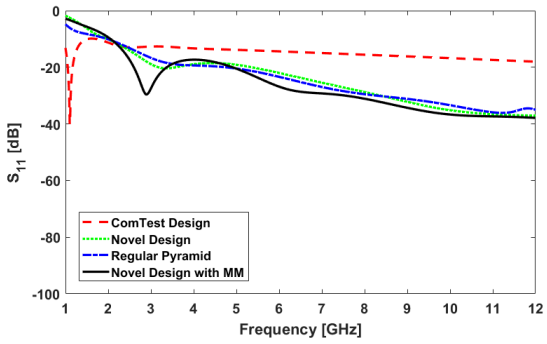

(d) Incidence angle $\theta = 45^{\circ}$.

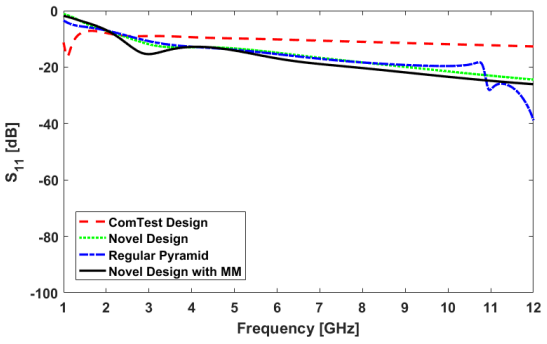

(e) Incidence angle $\theta = 60^{\circ}$.

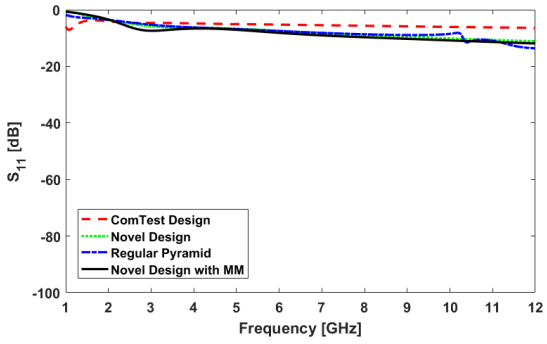

(f) Incidence angle $\theta = 75^{\circ}$.

Figure 3.13: S_{11} for different incidence angles.

The behavior of this novel design absorber can be analyzed using a horizontal and vertical plane analysis, changing θ and ϕ angles separately. Figure 3.14 shows the simulation result for horizontal plane analysis, and Figure 3.15 shows the simulation result for vertical plane analysis of this novel design with an MM unit cell base with the various angle of incidence (θ) and polarization (ϕ).

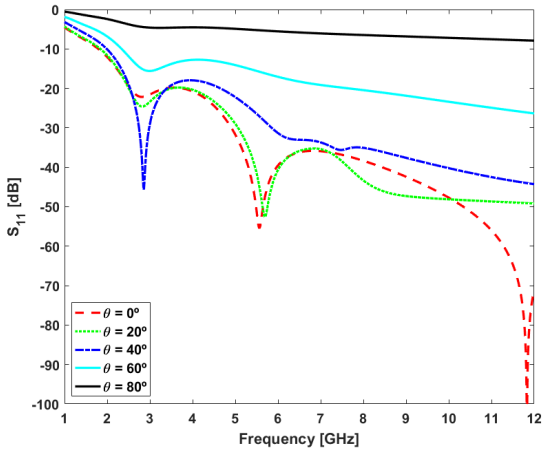

Figure 3.14: The S_{11} for horizontal plane of the Novel Design with MM Unit Cell for frequency range 1-12 GHz.

From Figure 3.14, it is observed that the maximum incidence angle that allows S_{11} levels under -20 dB for frequencies above 2 GHz is $\theta = 40°$.

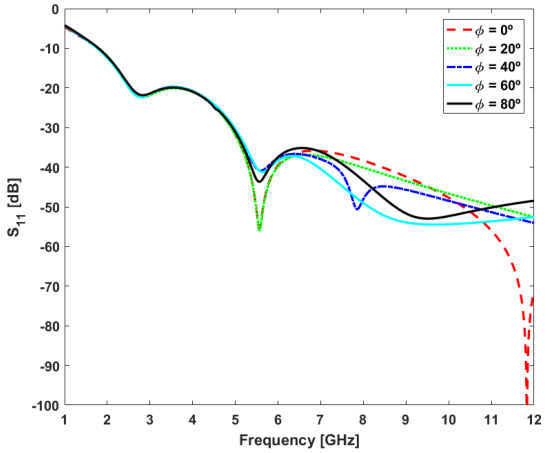

Figure 3.15: The S_{11} for vertical plane of the Novel Design with MM Unit Cell for frequency range 1-12 GHz.

From Figure 3.15, it is observed that this novel design is polarization insensitive and gives S_{11} almost less than -20 dB for frequencies above 2 GHz.

3.2.3 Radar Cross Section Analysis with MM

The RCS analysis of the proposed design uses an array of 10x10 unit cells, using an asymptotic solver for surveying the monostatic RCS. The resulting simulations for 1, 6 and 12 GHz frequencies are enough to understand the absorber's behavior for the proposed range. Figure 3.16 shows the 10x10 absorber array configuration with MM at the base.

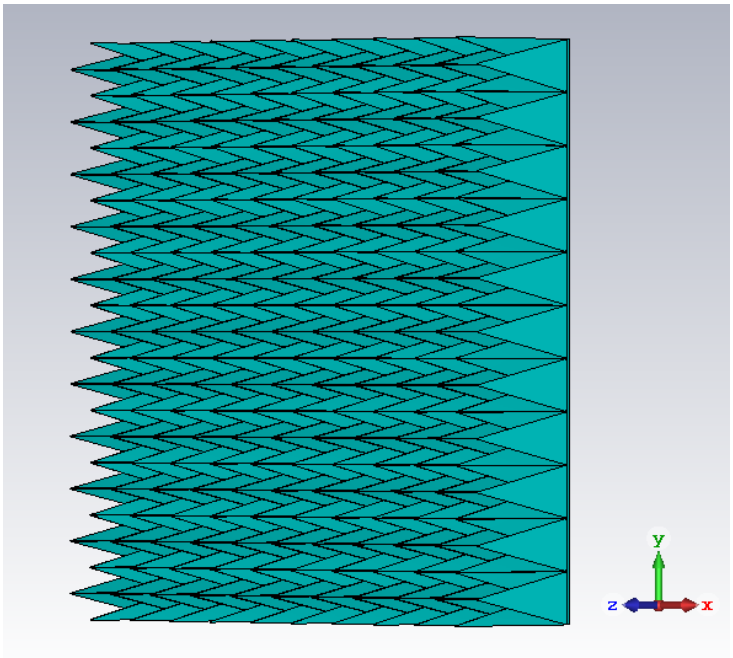

Figure 3.16: The 10 x 10 array of the proposed structure.

CST allows access to the observation rays, which show the EM waves scattered in the direction of interest. As the scale in the top right corner shows, a blue observation reflected ray means that the incident ray is almost totally absorbed as the reflected ray presents a low EM intensity value (0,03 V/m). On the other hand, a red observation reflected ray means that the incident ray has been reflected with a total EM intensity value (1 V/m). Figure 3.17 illustrates the observation rays showing the reflected waves for normal incidence.

As the Figure 3.17 shows, this absorber array has absorbed almost all the incident rays, as the observation rays have lower EM field intensity.

Figure 3.18 shows the RCS of the array of the proposed structure for 1, 6 and 12 GHz. The RCS of the proposed design is within -40 dB throughout the angle of incidence θ, which is a good figure of merit.

The proposed absorber performs better than the carbon-loaded polystyrene absorbers, which operate from 70 MHz to 110 GHz, as reported by ComTest. It serves almost the same S_{11} as the pyramidal-shaped absorber for the 1 to 6 GHz frequency range.

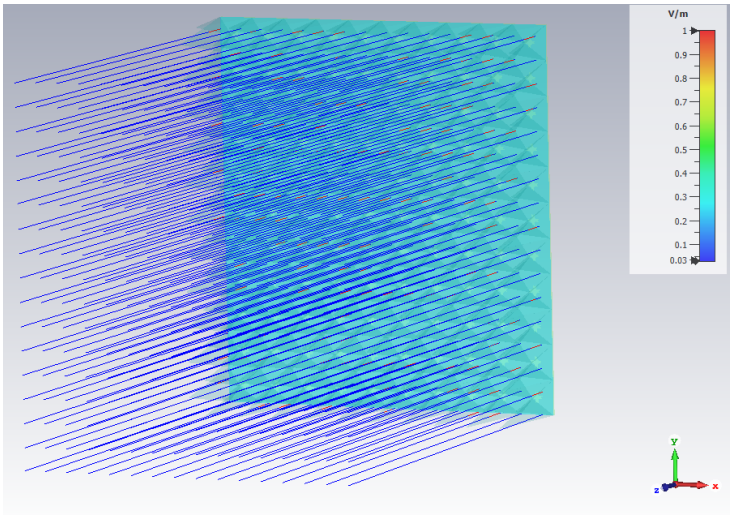

Figure 3.17: The 10 x 10 array of the proposed structure observed rays.

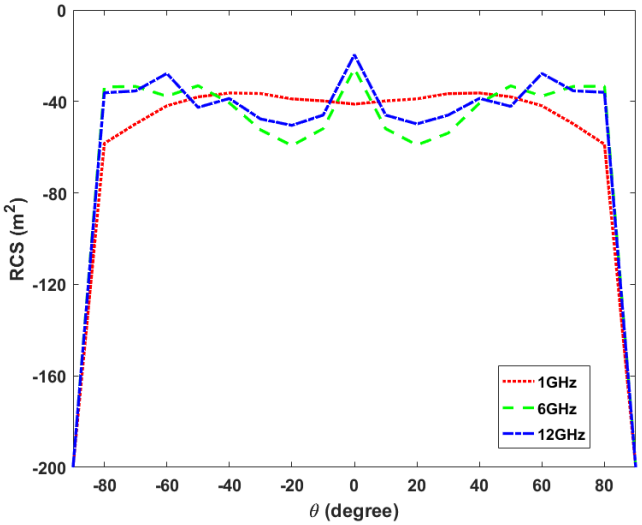

Figure 3.18: The RCS of the array of the proposed structure for 1, 6, and 12 GHz.

3.3 Laboratory Measures on Absorber Material

As part of absorber study and comprehension, laboratory tests on absorber material were performed and are essential to understanding the effect of using different types of material and incidence angles. This section presents some laboratory results on the two absorber materials that are the most used, polyurethane foam and polystyrene material. Due to production delays, it was impossible to test the MM simulated previously. Figure 3.19 presents the environment of the test inside a AC at IT Aveiro covered with walls covered with ComTest polystyrene absorber material.

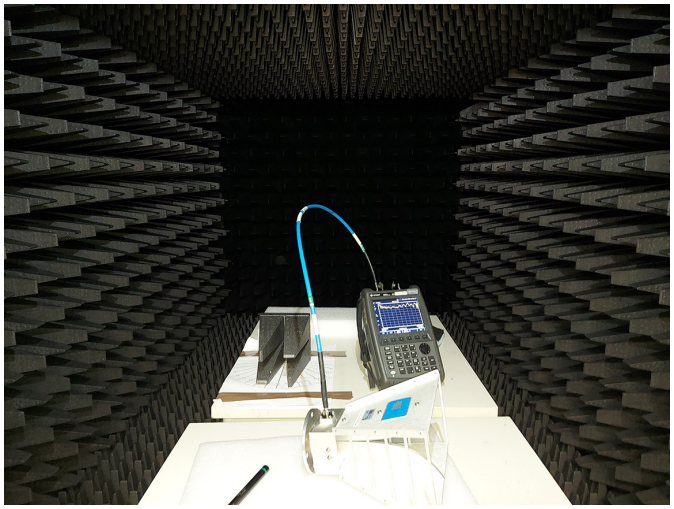

Figure 3.19: Laboratory test environment, inside IT Aveiro anechoic chamber.

The material list starts with a Keysight N9918A FieldFox handheld microwave analyzer, as illustrated in Figure 3.20 [56].

Figure 3.20: Keysight N9918A FieldFox Handheld Microwave Analyzer, 26.5 GHz

The antenna type chosen to perform the analysis was an A-Info LB-7180-NF broadband horn antenna with a frequency range from 0.7 GHz to 18 GHz with 12 dBi gain and N-Type female cable connection, as shown in Figure 3.21 [57].

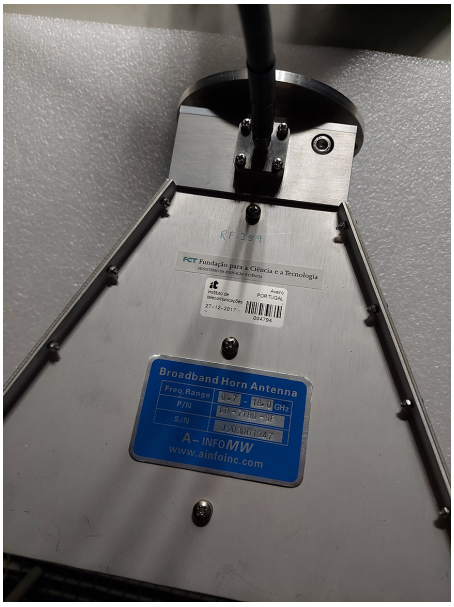

Figure 3.21: Broadband Horn Antenna with frequency range from 0.7 GHz to 18 GHz.

Before connecting the antenna to the microwave analyzer, it is mandatory to calibrate it using a Keysight calibration kit depicted in Figure 3.22 to avoid wrong data analysis.

Figure 3.22: Keysight Calibration Kit.

3.3.1 Polyurethane Foam Material

The first S_{11} analysis is for a carbon-loaded polyurethane material using two horn antennas and a smooth piece of absorber material with approximate dimensions (L x W x H): 120 x 60 x 2 cm^3, as shown in Figure 3.23. The absorber is placed over a table with a printed protractor to configure the desired angle. The distance between the absorber material and the antennas is about 60 cm. The antenna on the left is responsible for the wave emission, and the antenna on the right is responsible for the wave reception.

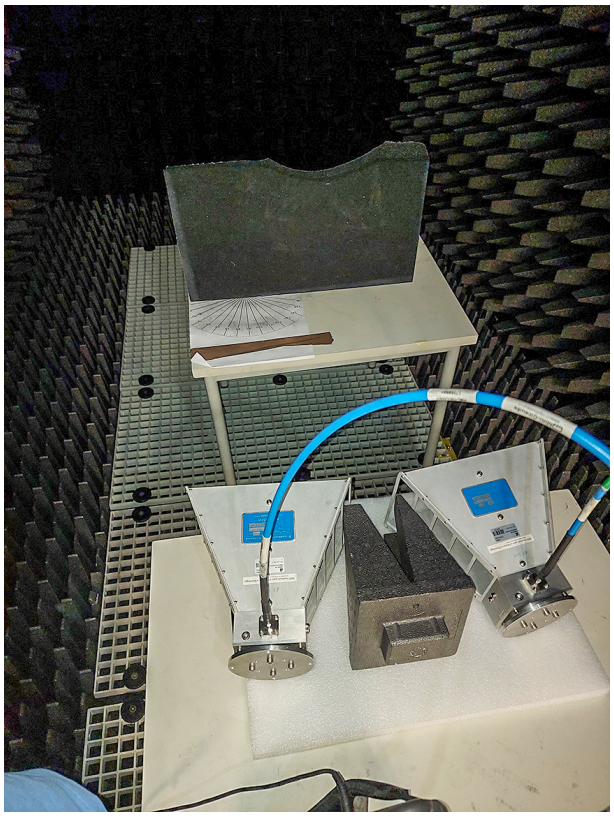

Figure 3.23: S_{11} test environment using carbon-loaded polyurethane foam.

The measurements were performed for vertical and horizontal planes, corresponding to the transmitter and receiver in horizontal and vertical positions. The results are shown in Figure 3.24 and Figure 3.25 respectively.

From Figure 3.24, representing the vertical plane result, it is clear that as the θ angle increases, the S_{11} decreases its absolute value, translating into a worse absorption rate of the absorber. The difference of the S_{11} achieves 30 dB between $\theta = 0°$ and $\theta = 80°$. As the frequency increases, the S_{11} increases its absolute value by 20 dB. This fact can be justified by the absorber performance increasing at higher frequencies.

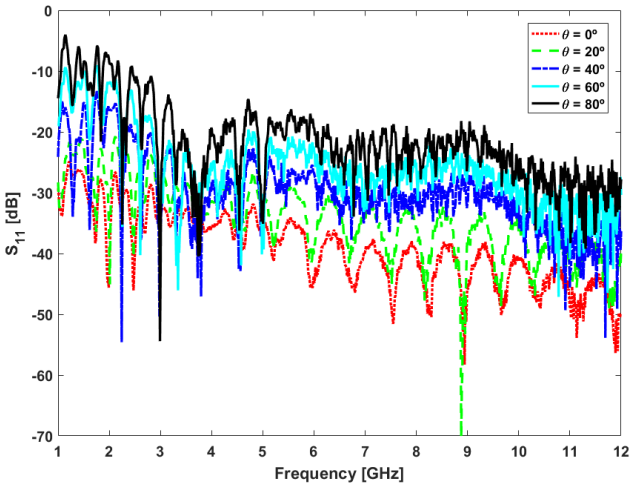

Figure 3.24: S_{11} test with Carbon-Loaded Polyurethane Foam material for the vertical plane.

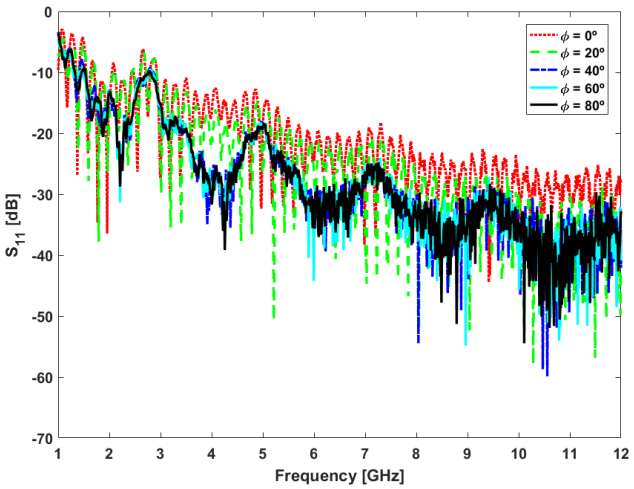

Figure 3.25: S_{11} test with Carbon-Loaded Polyurethane Foam Material for the horizontal plane.

Figure 3.25 shows a different plane perspective, with the ϕ angle changes, representing the horizontal plan. Increasing the ϕ angle in this plane does not produce a significant effect with less impact than the θ variation. The difference in this case from the farthest angles is less than 10 dB. As seen in the θ variation, as the frequency rises, the absorber performance increases also.

3.3.2 Polystyrene ComTest MT45 Material

The second S_{11} analysis is for a ComTest MT45 Polystyrene material with approximate dimensions of (L x W x H): 120 x 60 x 20 cm^3, using two horn antennas as shown in Figure 3.26. The distance between the absorber material and the antennas is 60 cm, and the antenna arrangement is the same as in the previous analysis with carbon-loaded urethane foam.

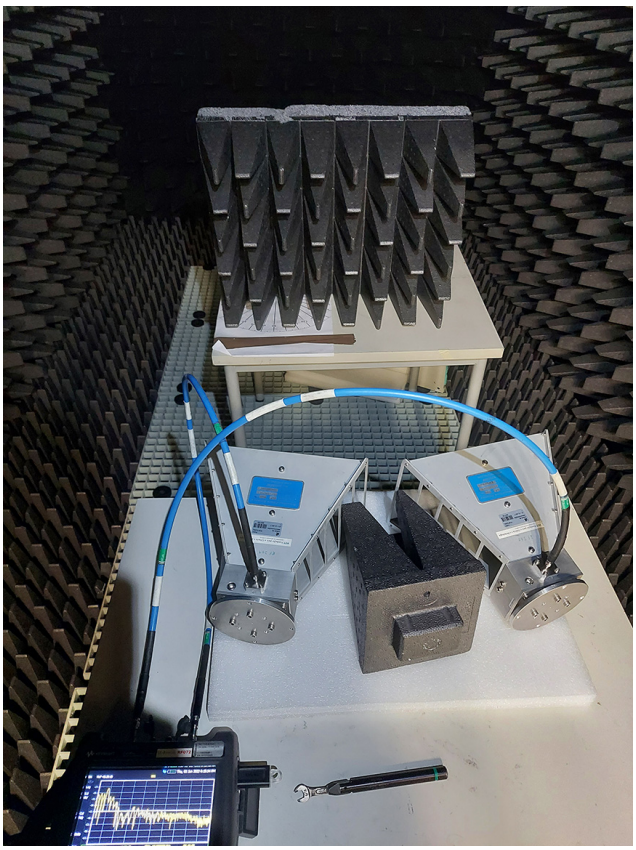

Figure 3.26: S_{11} test environment using ComTest MT45 Polystyrene material.

From Figure 3.27, representing the vertical plane analysis, the θ angle change results in the same S_{11} variation as the previous analysis. As the incident angle increases to its maximum, the S_{11} increases by about 30 dB between $\theta = 0°$ and $\theta = 80°$. The performance of the ComTest MT45 is slightly better than the carbon-loaded urethane foam for about 7 dB of S_{11}.

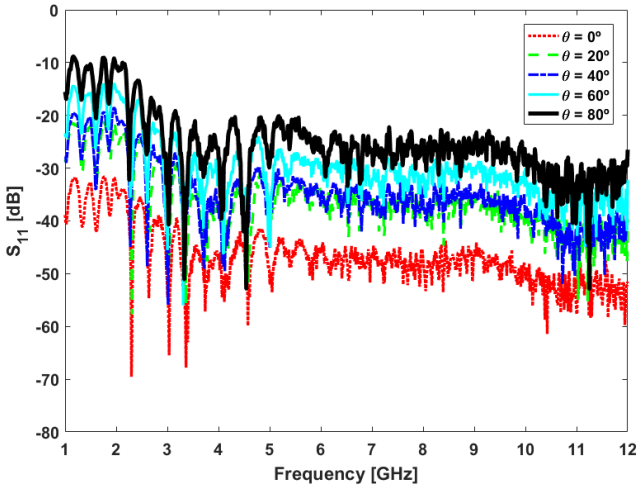

Figure 3.27: S_{11} test with ComTest MT45 Polystyrene Material with the antenna in vertical plane.

For the horizontal plane, illustrated in Figure 3.28, the result does not follow the result obtained for the carbon-loaded urethane foam.

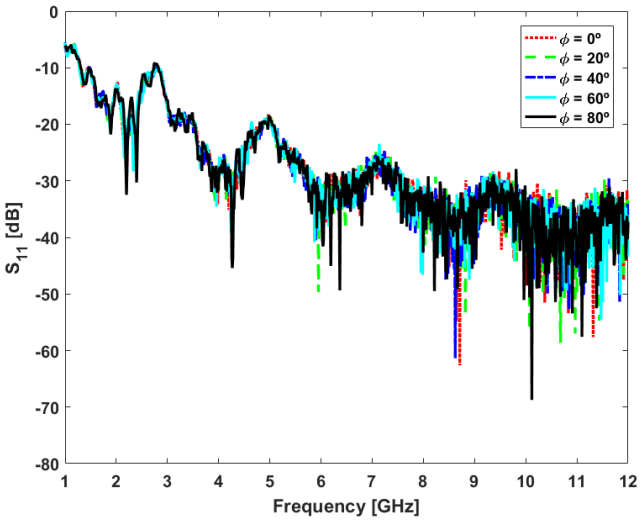

Figure 3.28: S_{11} test with ComTest MT45 Polystyrene Material with the antenna in horizontal plane.

In this representation, varying the ϕ angle does not impact the S_{11} as the performance is almost identical for all tested angles, following the performance of the higher ϕ angles of the carbon-loaded foam. An explanation for this effect could be the arrangement of the absorber tips that could provide immunity to the ϕ variations.

4

Characterization of the Anechoic Chamber with different Absorber Material

Contents

This chapter presents the AC characterization using CST Microwave Studio to compare different absorber materials covering the AC. The goal is to study the radiation pattern and gain produced by antennas inside each AC and compare the results with the free space.

4.1 Anechoic Chamber Simulation Scenario

For the simulation scenario an compact AC was built with a size of (L x W x H): 0.4 x 0.4 x 0.3 m^3, as shown in Figure 4.1.

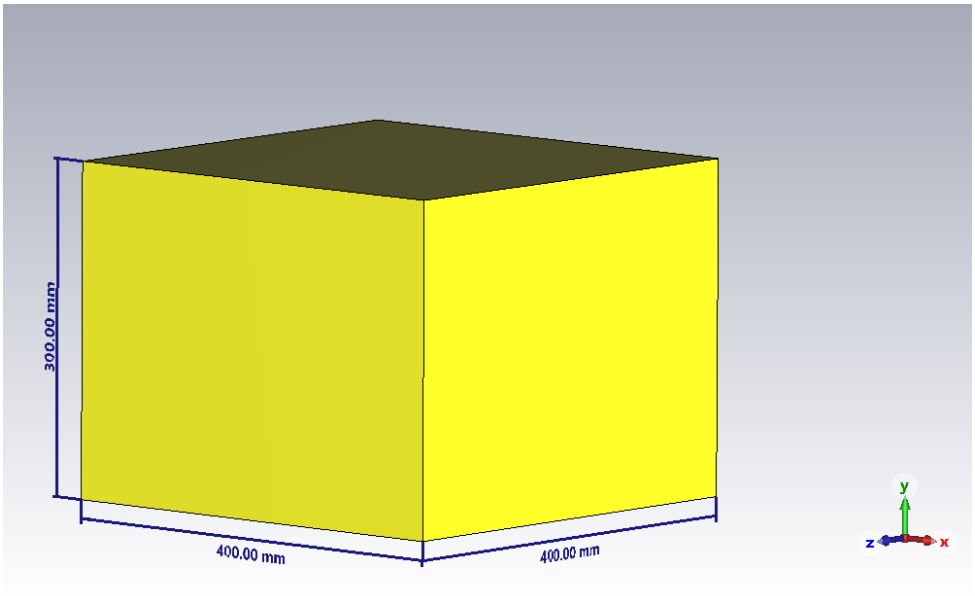

Figure 4.1: Anechoic Chamber with dimensions.

The chamber has a thin metal cover protection of 1 mm to provide an EM shield. The metal chosen for this chamber was pure copper. The primary purpose is to control external radiation penetration that can spoil the interior environment and prevent the inside radiation from leaving the chamber, increasing the absorptivity, as seen in the previous chapter.

Two types of microwave absorbers, already studied in this dissertation, will be applied, the first is a conventional pyramidal absorber material, and the second is a MM absorber. The purpose is to achieve an AC which can provide a simulated free space environment in a compact space. The antennas used in these studies will be a patch antenna for 2.92 GHz and a monopole antenna for 3 GHz.

Usually, tested antenna are placed with a minimum λ distance from the closest wall, however, due to the small chamber size, the standard is to put the antenna between the $\frac{\lambda}{4}$ and the $\frac{\lambda}{2}$ distance from the closest wall.

4.2 Gain Analysis using a Monopole Antenna

The 3D radiation pattern and gain of a monopole antenna in free space is a reference for comparing each tested chamber's capability to provide a free-space environment. The monopole antenna that will perform the tests has a resonating frequency of around 3 GHz, as illustrated in Figure 4.2.

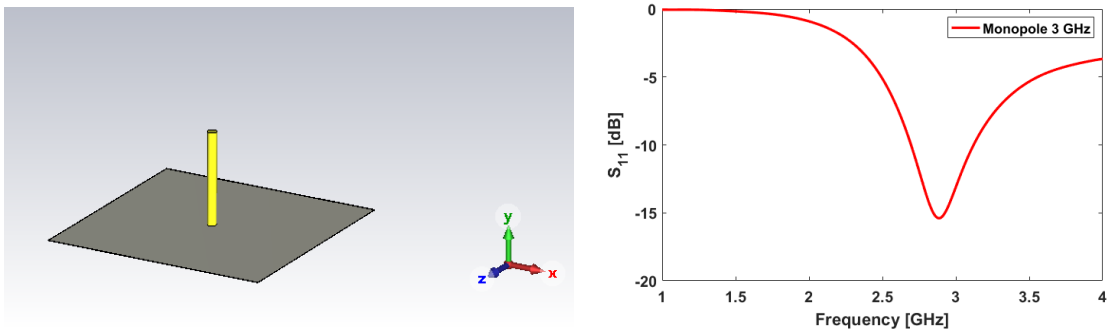

(a) Monopole Antenna. **(b)** S_{11} of the Monopole Antenna.

Figure 4.2: Monopole Antenna and respective S_{11}.

The results obtained in free space are the base for comprehending the absorber's performance in the following chamber analysis. For the 3 GHz frequency the observed gain and 3D-radiation pattern are illustrated in Figure 4.3.

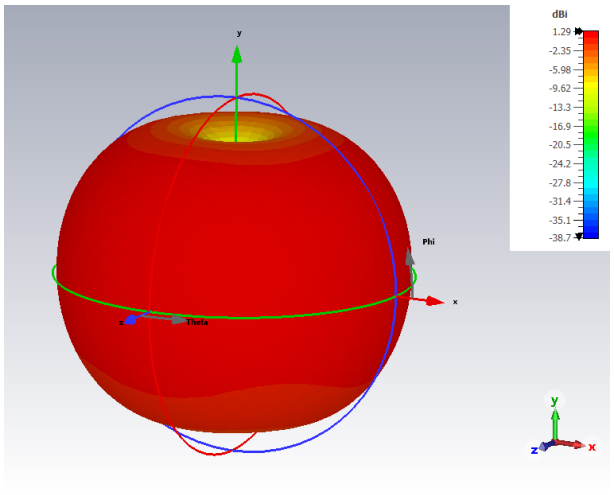

Figure 4.3: Monopole antenna gain for a frequency of 3 GHz at free space.

As shown in Figure 4.3, the maximum gain of this antenna for 3 GHz is about 1.29 dBi, establishing a reference gain that this antenna has to achieve for this frequency inside an AC.

For a far-field analysis, the antenna has to be at a far-field distance as mentioned in section 2.5.1. As the lower frequency is 3 GHz, the correspondent wavelength is 10 cm, and the D of the antenna is 2.5 cm, so the resulting R distance has to be at a much greater distance than the correspondent wavelength. The antenna is placed at $\frac{\lambda}{4}$, 2.5 cm, from the closest wall due to the chamber's small size, which only satisfies eq. (2.2).

The first AC tested is illustrated in Figure 4.4, and was covered with MM absorber.

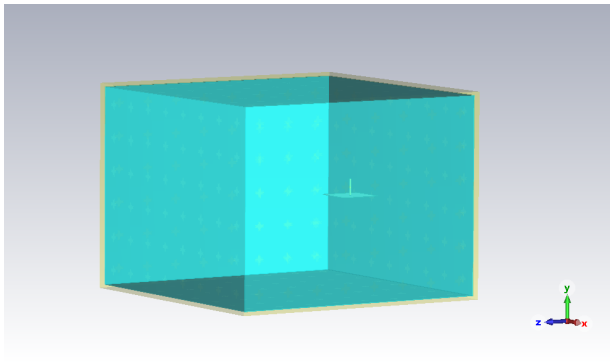

Figure 4.4: Anechoic Chamber with MM absorber.

Proceeding with the simulation after assembling the MM absorber in the chamber, the result for 3 GHz is presented in Figure 4.5.

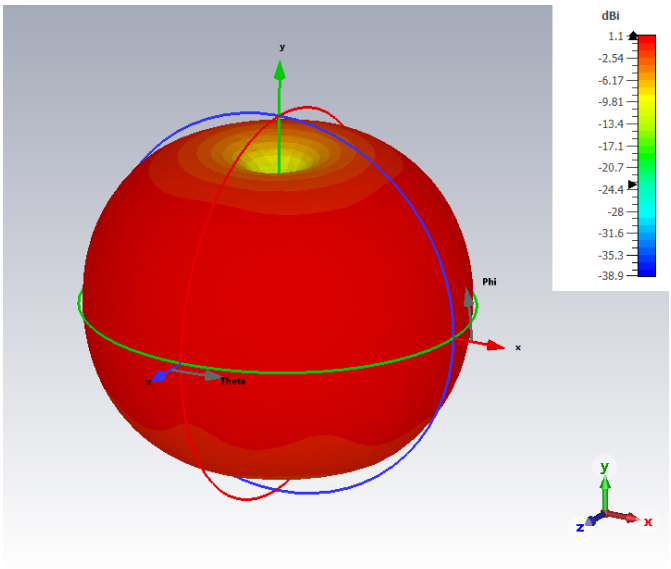

Figure 4.5: Monopole antenna gain for a frequency of 3 GHz inside Anechoic Chamber with MM absorber.

For a frequency of 3 GHz, the gain difference compared with the free space simulation has decreased by 0.19 dB, with a maximum gain of 1.1 dBi. The 3D radiation pattern is faithful to the free space.

The second AC tested, illustrated in Figure 4.6, was covered with the novel absorber design showed in Figure 3.5 of chapter 3.

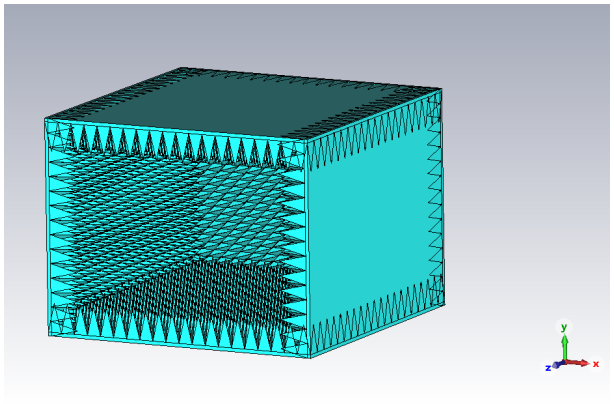

Figure 4.6: Anechoic Chamber with a Novel Design absorber.

The novel absorber covering the chamber has a height of 45 mm, 44 mm higher compared with only the MM. The simulation result for 3 GHz with this material inside the chamber is shown in Figure 4.7.

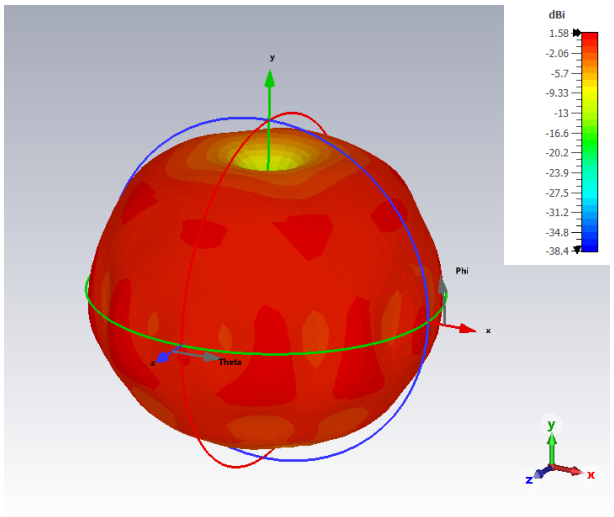

Figure 4.7: Monopole antenna gain for a frequency of 3 GHz inside Anechoic chamber with a Novel design absorber.

For the 3 GHz frequency, the difference of the gain compared with the free space simulation has increased by 0.29 dB and by 0.38 dB compared with the chamber covered with MM absorber, with a maximum gain of 1.58 dBi. The 3D radiation pattern is not so faithful to the free space as seen in the previous test. The MM material design has better performance than the conventional absorber material, as the radiation pattern is closer to the free space.

4.3 Gain Analysis using a Patch Antenna

In this test, the gain of a coaxial-feed rectangular patch antenna in free space is a reference for comparing each tested chamber's capability to provide a free-space environment. The patch antenna that will perform the tests has a resonating frequency of around 2.92 GHz, as illustrated in Figure 4.8.

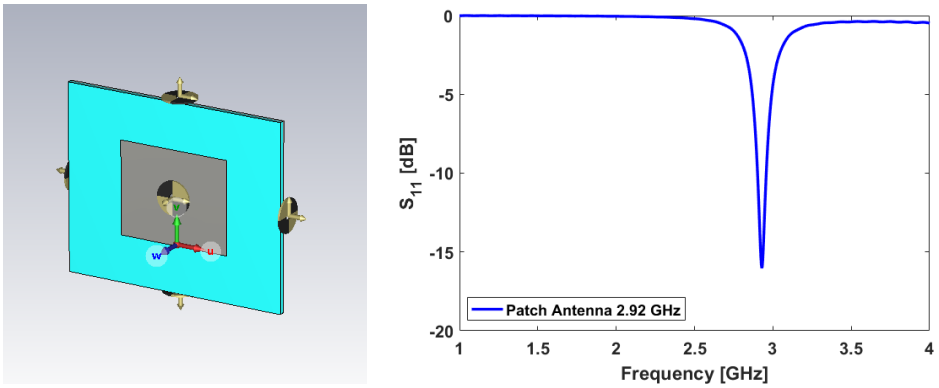

(a) Patch Antenna. **(b)** S_{11} of the Patch Antenna.

Figure 4.8: Patch Antenna and respective S_{11}.

The results obtained in free space are the base for understanding the absorber's performance in the following chamber analysis. The observed gain and the 3D radiation pattern of this antenna are illustrated in Figure 4.9 for the resonating frequency around 2.92 GHz.

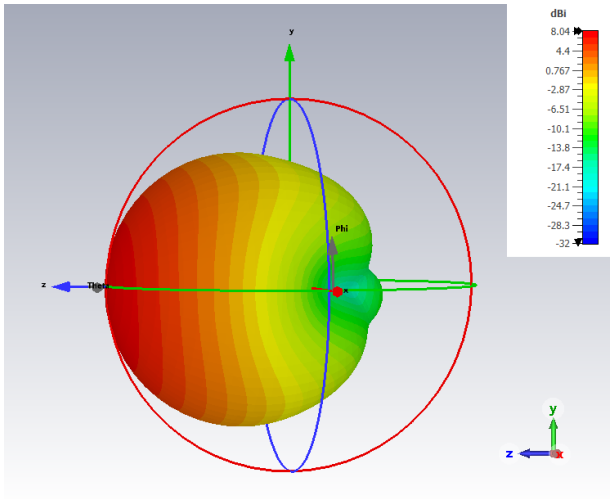

Figure 4.9: Free Space Radiation Pattern for Patch Antenna.

As shown in Figure 4.9, the maximum gain of this antenna for 2.92 GHz is about 8.04 dBi, establishing

a reference gain and 3D radiation pattern that this antenna has to follow for this frequency inside an AC.

For a far-field analysis, the antenna has to be at a far-field distance as mentioned in section 2.5.1. As the lower frequency is 2.92 GHz, the correspondent wavelength is 10.26 cm, and the D of the antenna is 10 cm, so the resulting R distance has to be greater than 19.5 cm. The antenna is placed at $\frac{\lambda}{4}$, 2.7 cm, from the closest wall due to the chamber's small size.

The first AC tested is illustrated in Figure 4.10, and was covered with MM absorber.

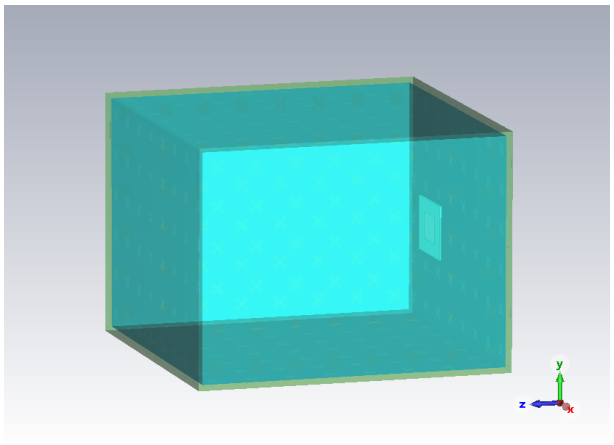

Figure 4.10: Anechoic Chamber with MM absorber material and Patch Antenna.

Continuing with the simulation after assembling the MM absorber in the chamber, the result for 2.92 GHz is presented in Figure 4.11.

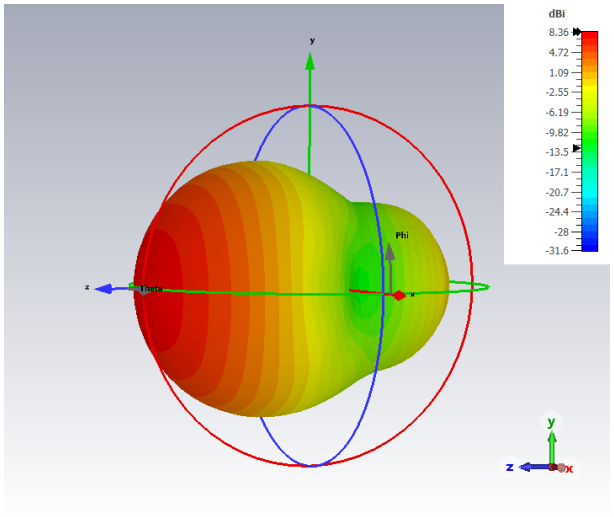

Figure 4.11: Anechoic Chamber with MM absorber material Radiation Pattern for Patch Antenna.

For a frequency of 2.92 GHz, the gain difference compared with the free space simulation has increased by 0.32 dB, with a maximum gain of 8.36 dBi. The 3D radiation pattern remains faithful to the

free space analysis.

The second AC tested, illustrated in Figure 4.12, was covered with the novel absorber design shown in Figure 3.5 of chapter 3.

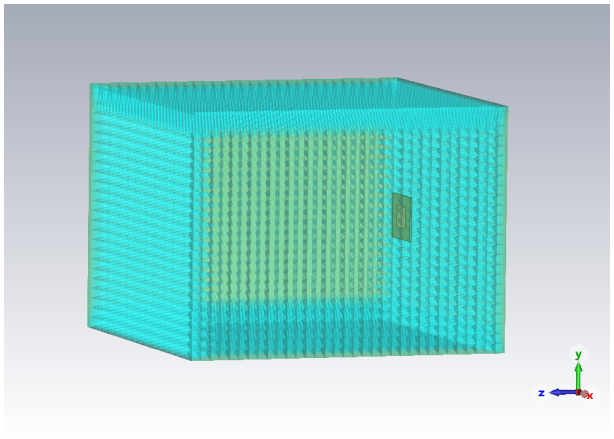

Figure 4.12: Anechoic Chamber with Conventional Pyramid absorber material and Patch Antenna.

The absorber covering the chamber has a height of 45 mm, 44 mm more when compared with only the MM. The simulation result for a frequency of 2.92 GHz with this material inside the chamber is shown in Figure 4.13.

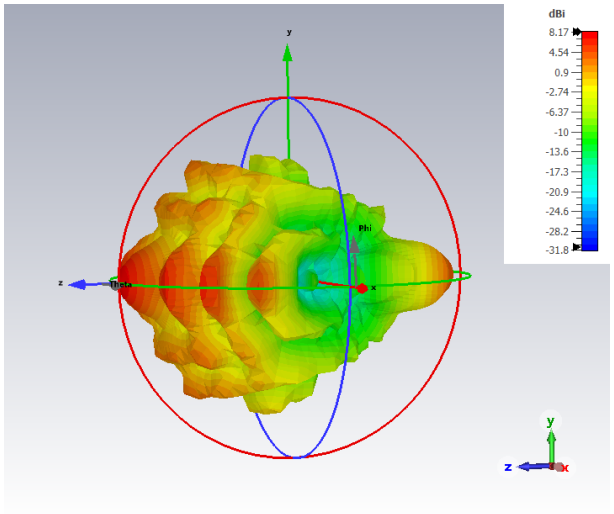

Figure 4.13: Anechoic Chamber with Conventional Absorber Material Radiation Pattern for Patch Antenna.

For the 2.92 GHz frequency, the difference in gain compared with the free space simulation has increased by 0.13 dB and decreased by 0.19 dB compared with the chamber covered with MM absorber, with a maximum gain of 8.17 dBi. The 3D radiation pattern is not faithful to the free space analysis, showing unacceptable discrepancies. The MM material design has shown better performance than the

novel design as the radiation pattern is closer to the free space than the conventional absorber material.

These simulations can demonstrate the AC performance by comparing the 3D radiation pattern and free space gain of the monopole antenna. The MM material shows promising results and can be an alternative for conventional absorbers. From another perspective, the space saved by MM can be an advantage in compact chamber design.

5

Conclusion

Contents

5.1 Summary

The main goal of this dissertation was to study the absorber materials and develop an innovative design absorber to contend with the traditional designs. The aim of an ideal AC is to provide an environment to obtain accurate results, identical to free space, in the smallest area, keeping the cost as low as possible without losing the quality of the measurements. The goal is to develop a design that can avoid high costs by using less absorber material than needed, increasing the chamber inside available space. The usage of RF absorber is crucial to avoid reflected waves from reaching QZ with higher power levels than the direct path wave, and the reflected waves have to arrive at the QZ with at least -30 dB or lower power than the direct wave.

In chapter 2, it was possible to understand the absorber materials basics and their advantages covering the ACs. The EM field measurement includes the measurements of antenna parameters, radiated emissions, radiated susceptibility, EMC, and RCS measurement. This chapter has represented the most used types of ACs and absorber materials. The final part of this chapter, one of the most important in this research, was the study of the state-of-the-art portfolio to collect relevant aspects to learn more about the absorber design and material properties. The knowledge from other authors increased the perspective to explore more solutions in this dissertation. The most used AC for a range between 0.7 GHz and 18 GHz, which is cheap and efficient, is the rectangular type AC. The chamber size changes with the lowest frequency tested.

The subsequent phase, chapter 3, was the starting point for the characterization of traditional absorber design simulations using CST Studio. The pyramidal proves to be the best design to use, facing up with other forms, with the best S_{11} result for the proposed frequency range. It was possible to change the structure of the absorber, observing the effects of the modifications and allowing the research for a better absorber design solution. A new MM design was developed in this chapter, using the information acquired from chapter 2. The chosen design was based on a Portuguese medal designated ”Grã Cruz” providing good S_{11} results in simulations tests. The chapter ends with performed laboratory measures inside IT AC used to visualize the absorber performance differences between the ComTest and the traditional foam materials. ComTest absorber material has shown immunity to the Φ variations, unlike the urethane foam.

Chapter 4 describes the assembled absorber materials inside a compact chamber to test their performance. The MM showed satisfactory results, close to the free space, remembering that the thickness of this material is about 1 mm. The results of the conventional absorber were not so good as the MM, showing worse results. Concluding that compact chambers were only possible using MM absorber due to the reduced available interior space.

Considering all the developed work and the obtained results, it is important to highlight some conclusions. Without an absorber, there is no AC due to high reflections inside. The absorber’s composition

is usually carbon-loaded materials, such as polyurethane or polystyrene foams. They can be found in wedge or pyramidal shapes to help the absorber impedance match with free space impedance. The absorber's size depends on the chamber's operating frequency, and the measure follows the lower operating frequency. The pyramidal is the most reliable structure to use as an absorber due to its high performance showing lower S_{11} values compared with other designs. Using the data provided by the simulations, a new absorber design was developed, using successful materials used by other researchers, presented in the state-of-the-art. The MMs is the secret weapon of absorber material development and can be easily changed to meet the requirements of a specific project. A novel absorber design achieved better performance than the conventional pyramid design for a frequency range above 10 GHz. Although, the performance was not suitable for lower frequencies than the traditional format. The new MM design developed obtained better performance for higher frequency due to its layer disposition and material properties.

5.2 Future Work

Considering the planned future work under the scope of this study, there are some improvements to reach in several absorber material and chamber aspects. Some articles related to developments of corner absorbers claim a significant reflection reduction inside the AC. This absorber type was not developed in this dissertation and can be part of a future work list.

Another task is to improve or create a novel design based on the pyramidal shape or study other geometric forms that can achieve better results for the lower frequencies and, at the best hypothesis, saving also space.

For the higher frequencies, perform MM research, choosing other material layer compositions, exploring the top layer pattern following the best-researched uses, and, if possible, improving them.

With an improved absorber, try to reduce the size of the AC to allow portability and a high-frequency test range with the lowest reflections possible to provide a free space environment occupying less space.

Bibliography

[1] 3DS, “CST Studio,” last Accessed on 01/03/2022. [Online]. Available: https://www.3ds.com/products-services/simulia/products/cst-studio-suite/

[2] IEEE, *IEEE Standard Definitions of Terms for Radio Wave Propagation IEEE Antennas and Propagation Society IEEE Standard Definitions of Terms for Radio Wave Propagation*. IEEE, 2014, vol. 145-2013, no. 2013.

[3] J. D. Kraus, *Antennas*, 2nd ed. New York: McGraw Hill Inc, 1997.

[4] W. H. Emerson, “Electromagnetic Wave Absorbers and Anechoic Chambers Through the Years,” *IEEE Transactions on Antennas and Propagation*, vol. 21, no. 4, pp. 484–490, 1973.

[5] W. H. Kummer and E. S. Gillespie, “Antenna Measurements—1978,” *Proceedings of the IEEE*, vol. 66, no. 4, pp. 483–507, 1978. [Online]. Available: http://ieeexplore.ieee.org/document/1455209/

[6] V. Rodriguez, *Anechoic Range Design for Electromagnetic Measuremnts*. London/Boston: Artech House Publishers, 2019.

[7] P. Society, *IEEE Standard Definitions of Terms for Radio Wave Propagation IEEE Antennas and Propagation Society IEEE Standard Definitions of Terms for Radio Wave Propagation*. IEEE, 2018, vol. 2013.

[8] W. T. Slayton, “Design and Calibration of Microwave Antenna Gain Standards - William Slayton NRL Report 4433,” Naval Research Laboratory, Washington D.C, Tech. Rep., 1954.

[9] A. C. Newell, R. C. Baird, and P. F. Wacker, “Accurate Measurement of Antenna Gain and Polarization at Reduced Distances by an Extrapolation Technique,” *IEEE Transactions on Antennas and Propagation*, vol. 21, no. 4, pp. 418–431, 1973.

[10] A. G. Repjar, A. C. Newell, and D. T. Tamura, “Extrapolation Range Measurements for Determining Antenna Gain and Polarization,” Boulder, Colorado, p. 88, 1987.

[11] T. Enforcement and T. Committee, *STANDARDS IEEE Standard for the Performance of Down-the-Road Radar Used in*. IEEE, 2019.

[12] L. Hollis, J.S ; Lyon, T.J ; Clayton, *Microwave Antenna Measurements*. Atlanta, GA: Inc., Scientific Atlanta, 1985.

[13] A. C. Ludwig, "The Definition of Cross Polarization," *IEEE Transactions on Antennas and Propagation*, vol. 21, no. 1, pp. 116–119, 1973.

[14] P. J. Bevelacqua, "Cross Polarization Cross Polarization," p. 200, 2016, last Accessed on 15/12/2021. [Online]. Available: https://www.antenna-theory.com/definitions/crosspolarization.php

[15] TreLink Antenna, "What is Antenna Polarization," p. 1, 2018, last Accessed on 22/11/2021. [Online]. Available: https://www.trelink.com/what-is-antenna-polarization/

[16] D. Gray, "How to Choose an Antenna Range Configuration," *AMTA 24th Annual Meeting and Symposium*, p. 7, 2002.

[17] V. Rodriguez, "Basic Rules for Indoor Anechoic Chamber Design [Measurements Corner]," *IEEE Antennas and Propagation Magazine*, vol. 58, no. 6, pp. 82–93, dec 2016. [Online]. Available: http://ieeexplore.ieee.org/document/7762868/

[18] W. H. Emerson and H. B. Sefton, "An Improved Design for Indoor Ranges," *Proceedings of the IEEE*, vol. 53, no. 8, pp. 1079–1081, 1965.

[19] H. Stockman, "Communication by Means of Reflected Power," *Proceedings of the IRE*, vol. 36, no. 10, pp. 1196–1204, oct 1948. [Online]. Available: http://ieeexplore.ieee.org/document/1697527/

[20] L. H. Hemming, *Electromagnetic Anechoic Chambers*. IEEE, 2002. [Online]. Available: http://ieeexplore.ieee.org/xpl/bkabstractplus.jsp?bkn=5273701

[21] G. EMC, "Ferrite Tiles," last Accessed on 10/01/2022. [Online]. Available: https://globalemc.co.uk/components/ferrite-tiles/

[22] C. Holloway, R. DeLyser, R. German, P. McKenna, and M. Kanda, "Comparison of electromagnetic absorber used in anechoic and semi-anechoic chambers for emissions and immunity testing of digital devices," *IEEE Transactions on Electromagnetic Compatibility*, vol. 39, no. 1, pp. 33–47, 1997. [Online]. Available: http://ieeexplore.ieee.org/document/554693/

[23] E. Cuming, "Emerson and Cuming Absorber," last Accessed on 10/01/2022. [Online]. Available: https://www.ecanechoicchambers.com/

[24] H. Nornikman, P. Soh, A. Azremi, and M. Anuar, “Performance Simulation of Pyramidal and Wedge Microwave Absorbers,” in *2009 Third Asia International Conference on Modelling and Simulation*. IEEE, 2009, pp. 649–654. [Online]. Available: http://ieeexplore.ieee.org/document/5072063/

[25] D. Green and D. Smith, “Design, construction and performance of a small, low cost anechoic measuring system for research applications,” in *IEEE Antennas and Propagation Society International Symposium. 1995 Digest*, vol. 4. IEEE, 1995, pp. 1738–1741. [Online]. Available: http://ieeexplore.ieee.org/document/530919/

[26] A. Hasnain, M. Imran, Z. Rohaiza, S. Roslan, A. Takiyuddin, A. Rusnani, and A. Azremi, “Preliminary development of mini anechoic chamber,” in *2007 Asia-Pacific Conference on Applied Electromagnetics*. IEEE, dec 2007, pp. 1–5. [Online]. Available: http://ieeexplore.ieee.org/document/4603965/

[27] H. Abdullah, M. S. Sabilurrashad, I. M. Ibrahim, R. Ariffin, S. Z. A. Jalil, W. K. W. Ali, and M. N. Taib, “Design of portable mini anechoic chamber using low cost composite absorber,” in *2009 IEEE Student Conference on Research and Development (SCOReD)*, no. SCOReD. IEEE, 2009, pp. 526–528. [Online]. Available: http://ieeexplore.ieee.org/document/5442944/

[28] M. Winebrand, J. Aubin, and M. Boumans, “A two-level GTD utilization in designing anechoic chambers for antenna measurements,” *IEEE Antennas and Propagation Society, AP-S International Symposium (Digest)*, no. I, pp. 25–28, 2009.

[29] J. Aubin, M. Winebrand, and V. Vinogradov, “Experimental validation of the Two - Level GTD Method for design of anechoic chambers,” in *2011 IEEE International Symposium on Antennas and Propagation (APSURSI)*, no. L. IEEE, jul 2011, pp. 1893–1896. [Online]. Available: http://ieeexplore.ieee.org/document/5996869/

[30] R.-C. Liu, T.-H. Lee, and H.-T. Chou, “An innovative design of anechoic chamber for the EM radiation measurement at low frequencies,” in *2012 Asia Pacific Microwave Conference Proceedings*. IEEE, dec 2012, pp. 917–919. [Online]. Available: http://ieeexplore.ieee.org/document/6421777/

[31] P. Pinho, H. Santos, and H. Salgado, “Design of an anechoic chamber for w-band and mmwave,” *Electronics (Switzerland)*, vol. 9, no. 5, pp. 1–13, 2020.

[32] S. Suganthi, D. D. Patil, and E. Chand, “Integration of 0.1 GHz to 40 GHz RF and microwave anechoic chamber and the intricacies,” *Progress In Electromagnetics Research C*, vol. 101, no. October 2019, pp. 29–42, 2020.

[33] Z. Cai, Y. Zhou, L. Liu, Y. Qi, W. Yu, J. Fan, M. Yu, and Q. Luo, “Small Anechoic Chamber Design Method for On-Line and On-Site Passive Intermodulation Measurement,” *IEEE Transactions on Instrumentation and Measurement*, vol. 69, no. 6, pp. 3377–3387, 2020.

[34] S. K. N. Jameeu, I. H. Alve, M. A. Alam, A. Ahsun, M. T. Ali, and M. A. Rahman, “Mini Economical Anechoic Chamber,” *2020 IEEE Region 10 Symposium, TENSYMP 2020*, no. June, pp. 522–525, 2020.

[35] V. Rodriguez, “A cone shaped taper anechoic chamber for antenna measurements in the 200 MHz to 18GHz frequency range,” in *Proceedings of the 2012 IEEE International Symposium on Antennas and Propagation*. IEEE, jul 2012, pp. 1–2. [Online]. Available: http://ieeexplore.ieee.org/document/6348704/

[36] S. Zhang, D. Speight, A. Paraskevopoulos, D. Fonseca, C. Luxey, W. Whittow, and J. Pinto, “On-body measurements of embroidered spiral antenna,” *2015 Loughborough Antennas and Propagation Conference, LAPC 2015*, 2015.

[37] P. J. Bevelacqua, “SParameters,” p. 200, 2015, last Accessed on 25/01/2022. [Online]. Available: https://www.antenna-theory.com/definitions/sparameters.php

[38] T. A. Kuzmich, “Mathematical Modelling of Cone Shaped Tapered Anechoic Chamber,” *Conference Proceedings - 2019 Radiation and Scattering of Electromagnetic Waves, RSEMW 2019*, pp. 492–495, 2019.

[39] N. P. Balabuha, N. L. Menshikh, A. D. Sakhno, and N. E. Shapkina, “Mathematical Simulating of Electromagnetic Field in the Quiet Zone of Pyramidal and Conical Tapered Anechoic Chambers: Comparison of Results,” *Progress in Electromagnetics Research Symposium*, vol. 2021-November, pp. 2552–2561, 2021.

[40] V. Rodriguez, “Analysis of the Quiet Zone of Tapered Chambers,” *2021 IEEE International Symposium on Antennas and Propagation and North American Radio Science Meeting, APS/URSI 2021 - Proceedings*, pp. 1729–1730, 2021.

[41] B. K. Chung and H. T. Chuah, “Design and Construction of a Multipurpose Wideband Anechoic Chamber,” *IEEE Antennas and Propagation Magazine*, vol. 45, no. 6, pp. 41–47, 2003.

[42] A. Farahbakhsh and M. Khalaj-Amirhosseini, “Using Metallic Ellipsoid Anechoic Chamber to Reduce the Absorber Usage,” *IEEE Transactions on Antennas and Propagation*, vol. 63, no. 9, pp. 4229–4232, 2015.

[43] A. Farahbakhsh and D. Zarifi, “Analysis and design of metallic parabolic anechoic chamber,” *2017 11th European Conference on Antennas and Propagation, EUCAP 2017*, pp. 3053–3056, 2017.

[44] R. C. Johnson, H. A. Ecker, and R. A. Moore, “Compact Range Techniques and Measurements,” *IEEE Transactions on Antennas and Propagation*, vol. 17, no. 5, pp. 568–576, 1969.

[45] R. C. Liu and C. H. Li, “A Novel Design of Compact Antenna Test Range for Ultra-Precise Antenna Test,” *15th European Conference on Antennas and Propagation, EuCAP 2021*, 2021.

[46] S. F. Gregson and C. G. Parini, “A Parabolic Torus Compact Antenna Test Range for 5G NR Massive MIMO OTA Multi-User Test Applications,” *2020 IEEE International Symposium on Antennas and Propagation and North American Radio Science Meeting, IEEECONF 2020 - Proceedings*, pp. 1751–1752, 2020.

[47] A. Jernberg, M. Pinkasy, G. Pinchuk, T. Haze, R. Konevky, L. Shmidov, R. Braun, A. Giacomini, L. J. Foged, G. Baran, and M. Boumans, “Compact Antenna Test Range with New Shorter Focal Length for Heavy Duty Antenna Measurements,” *13th European Conference on Antennas and Propagation, EuCAP 2019*, no. EuCAP, pp. 5–9, 2019.

[48] P. Iversen, M. Boumans, and S. Burgos, “Mini compact range for automotive radar antenna testing,” *Proceedings of 6th European Conference on Antennas and Propagation, EuCAP 2012*, pp. 2240–2243, 2012.

[49] H. Wakatsuchi, J. Paul, and C. Christopoulos, “Performance of customizable cut-wire-based metamaterial absorbers: Absorbing mechanism and experimental demonstration,” *IEEE Transactions on Antennas and Propagation*, vol. 60, no. 12, pp. 5743–5752, 2012.

[50] H. Jiang, W. Yang, R. Li, S. Lei, B. Chen, H. Hu, and Z. Zhao, “A Conformal Metamaterial-Based Optically Transparent Microwave Absorber with High Angular Stability,” *IEEE Antennas and Wireless Propagation Letters*, vol. 20, no. 8, pp. 1399–1403, 2021.

[51] S. Ponnekanti, F. S. Al Khaled, and S. Sali, “An effective optimization method for the design of broadband microwave absorbers,” *International Journal of Numerical Modelling: Electronic Networks, Devices and Fields*, vol. 8, no. 6, pp. 447–454, 1995.

[52] N. I. Landy, S. Sajuyigbe, J. J. Mock, D. R. Smith, and W. J. Padilla, “Perfect metamaterial absorber,” *Physical Review Letters*, vol. 100, no. 20, pp. 1–4, 2008.

[53] S. Lai, Y. Guo, G. Liu, Y. Liu, C. Fu, H. Chang, Y. Wu, and W. Gu, “A High-Performance Ultra-Broadband Transparent Absorber With a Patterned ITO Metasurface,” *IEEE Photonics Journal*, vol. 14, no. 3, pp. 1–7, 2022.

[54] W. Zhu, I. D. Rukhlenko, F. Xiao, and M. Premaratne, “Polarization conversion in U-shaped chiral metamaterial with four-fold symmetry breaking,” *Journal of Applied Physics*, vol. 115, no. 14, 2014.

[55] F. Retardant and M. Absorber, “Eccosorb ® QR-13AF,” pp. 1–2, 2015. [Online]. Available: https://assets.lairdtech.com/home/brandworld/files/DSEccosorbQR-13AF.pdf

[56] Keysight, “Datasheet N9918A Fieldfox MW Analyzer,” p. 72, 2022. [Online]. Available: https://www.keysight.com/us/en/support/N9918A/fieldfox-a-handheld-microwave-analyzer-26-5-ghz.html

[57] AINFO, “LB-7180-NF Broadband Horn Antenna,” p. 1, 2022. [Online]. Available: https://www.ainfoinc.com/antenna-products/horn-antennas/broadband-horn-antennas/lb-7180-nf-broadband-horn-antenna-0-7-18-0-ghz-12db-gain-n-type-female